One fluid formulation for wave and structure interaction

Liang Yang

School of Mathematics, Computer Science & Engineering, City University London, EC1V 0HB, United Kingdom

Abstract

A simple and efficient computational framework is proposed for simulating of the wave interaction with rigid body, in the scope of immersed methods. Unlike existing publications, this method does not solve the general motion of rigid bodies in the Lagrangian form of Newton's law. Derived from the distributed Lagrange multiplier treatment of the rigid body, a new set of governing equations is presented on the fully Eulerian one-fluid formulation. To solve the problem numerically, the complex problem is separated into three parts: balance of the momentum and mass (dynamic problem), evolving of the Heaviside function by the external velocity (geometric problem) and rigid motion projection (kinematic problem). The conversation of mass and momentum are guaranteed by the multiphase fluid solver. The water, air and floating body coupling is accomplished by the smeared interface. A new way of initialisation and convection of the rigid Heaviside function is designed for an arbitrary shape. To deal with rigid velocity vector, a linear least square method is proposed. The excellent agreement between the numerical experiment and the reference data from experiemnts demonstrate the validity and applicability of the new methodology.

Keywords: One-fluid formulation, wave structure interaction, Heaviside initialisation and interpolation, linear least square projection, water impact

1. Introduction

The interaction between waves and structure is of great research interest in the naval and coastal engineering. A good understanding of such interaction is essential for the design of safe and high performance ships and civil engineering constructions such as offshore oil, gas platforms, wind farms and hydropower stations. The present paper is dedicated to the simulation of wave interaction with a rigid body through an immersed approach on a Cartesian grid, which will be outlined below.

Historically, the modelling of the interaction between the wave and rigid bodies has been developed via the numerical wave tank (NWT) method based

Email address: liang.yang.1@city.ac.uk (Liang Yang)

on the potential flow theory [1]. The Poisson equation in the non-viscous model is solved numerically by the Boundary Element Methods [1].The main disadvantage of these models is that they are unable to model the viscous effect and breaking waves.

The Navier-Stokes equations have been used more recently for the wave and floating bodies interaction problem [2, 3] to account for the viscous effect. Three different methodologies have been used for the numerical discretisation: particle based methods [3, 4], grid-based body fitted approaches [5, 6] and grid-based immersed methods [7, 8]. The Lagrangian particle methods can easily deal with the free surface and the impact problem, but the convergence rate and consistency of the algorithm are causes for concern, if the particles are the randomly perturbed [9]. Within the group of body fitted methodologies, the main disadvantage is the computational cost associated with the need for mesh updating or complete re-meshing, a factor particularly critical in the case of three-dimensional simulations. In this work, our focus is on the immersed type methods on a Cartesian grid, which have at least a first order convergence rate and an affordable computational cost.

Regarding the rigid body dynamics, there are three models used in common. First, the rigid body can be modelled via a very stiff continuum solid and solved by the immersed boundary method (IBM). The IBM was first introduced by Peskin [10] in 1972 to simulate the deformation of heart valves. A solid-to-fluid interpolated body force is added to the fluid to account for the presence of any immersed deformable solid. However, the modelling of a rigid body as a deformable case of a very stiff solid can lead to numerical instabilities [11] for the explicit method.

The traditional way of describing the rigid body dynamics via Newton-Euler formulation:

$$M\frac{\mathrm{d}\boldsymbol{u}_c}{\mathrm{d}t} = \boldsymbol{f}_c \qquad \text{translational motion} \tag{1a}$$

$$\boldsymbol{J}\frac{\mathrm{d}\boldsymbol{\omega}}{\mathrm{d}t} + \boldsymbol{\omega}\times\boldsymbol{J}\boldsymbol{\omega} = \boldsymbol{t}_c \qquad \text{rotational motion} \tag{1b}$$

where the M, $\boldsymbol{J}$ $\boldsymbol{\omega}$, $\boldsymbol{u}_c$, $\boldsymbol{f}_c$ and $\boldsymbol{t}_c$ are the mass, inertia tensor, angular velocity, centre mass velocity, force and torque applied on the rigid object, respectively. The fluid-rigid coupling is commonly achieved by a direct forcing approach [7, 12, 13, 14]. It introduces the Lagrangian coordinates for the rigid body and solves the additional set of Eq. (1). Several immersed techniques in conjunction with Newton-Euler formulation have been reported in 2D [15] and 3D [8, 16]. The main inconvenience of these methods is the necessity to solve the Newton's equation (1) and the additional algorithm to satisfy the kinematic and dynamic boundary conditions on the interface.

Some researchers have considered the rigid body as a fluid with kinetic constraints and open a door for the fluid-rigid body interaction problem. The first two methodologies that model a rigid region subject to a velocity constraint are the Distributed Lagrange-Multiplier/Fictitious-Domain (DLM) method of Patankar [17] and the Stress-Distributed Lagrange-Multiplier (Stress-DLM) of

Glowinski [18]. Both of these methods considered the rigid body to be of the same density as that of the underlying fluid. In general, these two DLM methods are solved in a weak manner with the help of an iterative Uzawa algorithm [17, 18], apparently shown to be very time consuming.

To avoid the formulation with a Lagrange multiplier, Patankar [19] proposed an alternative method for the direct approximation of the rigid velocity field. A projection procedure [19] is introduced in order to ensure the conservation of linear and angular momenta. The general advantage of these methods is the consideration of the rigid body dynamics in a Eulerian way, analogous to a fluid, facilitating the modelling of rigid and fluid coupling problems by means of the two-phase flow approach described above. In contrast with the previous direct forcing approach [8, 7, 13, 14], the inertias of the rigid body is fully accounted for the fluid solver. This method [7, 13, 20] have been applied to simulate single phase particulate flows or self-propelling immersed bodies. However, the Patankar's idea [19] on imposing the rigidity force is on a discrete level.

In this work, the rigid body governing equation with a rigidity force is written explicitly on a continuum level and proved to be equivalent to the Newton-Euler formulation (1). The new proposed formulation is applied to the wave interaction with a rigid floating body. In this way, the FSI problem is reformulated into a three-phases immersible flow problem, with a additional rigid motion constraint force. Then, it can be solved by the 'one-fluid' formulation for the multiphase flow [21, 22]. Solving the one-fluid formulation is proved to be equivalent for solving the separated set of equations with explicit enforcing the B.C.s.

The three different regions, water, air and structure, are represented by three Heaviside function. There is no Lagrangian particles/meshes introduced in the formulation, so the accuracy of this method is only depends on the discretisation scheme and approximation of the Heaviside function. We propose the convolution step to initialise the rigid Heaviside function for an arbitrary rigid shape and the high order interpolation step for the convection of the Heaviside function. The water-air interface is dealt with traditional Level Set technique.

Finally, a least square projection method is proposed purely from kinematics point of view in contrast with any existing work. There is no requirement for the integration of linear and angular momentum of the rigid region or necessarily knowing the mass and inertia tensor.

The structure of the paper is as follows. Section 2 describes briefly the fundamental three-phases Navier-Stokes equations for the wave interaction with a floating body problem. Section 3 describes the Level Set method used for representing the fluid and rigid body. Section 4 outlines the specific fluid solver used in this work, the classical fractional step method in conjunction with a Marker-and-Cell (MAC) spatial semi-discretisation scheme. In particular, it presents a novel methodology to project the rigid velocity from an arbitrary velocity field. Section 6 presents several two-dimensional numerical examples with the purposes of demonstrating the accuracy and flexibility of the new method. Finally, some conclusions will be summarised in the last section.

2. Problem description

2.1. Fluid mechanics

The incompressible viscous flow, occupying the domain Ω_f, which assumes to be an can be described in the spatial coordinates as,

$$\rho\left[\frac{\partial \boldsymbol{u}}{\partial t}+(\boldsymbol{\nabla u})\boldsymbol{u}\right]=-\boldsymbol{\nabla}p+\boldsymbol{\nabla}\cdot 2\mu\boldsymbol{D}(\boldsymbol{u})+\rho\boldsymbol{g} \qquad \text{in } \Omega_f \tag{2a}$$

$$\boldsymbol{\nabla}\cdot\boldsymbol{u}=0 \qquad \text{in } \Omega_f \tag{2b}$$

which represents the strong form of the incompressible Navier-Stokes equations, where $\boldsymbol{D}(\boldsymbol{u})=\frac{1}{2}(\boldsymbol{\nabla u}+(\boldsymbol{\nabla u})^T)$ is the strain rate tensor, ρ is the density field of the fluid and μ is the dynamic viscosity, $\boldsymbol{g}$ the gravitational acceleration respectively. With suitable initial/boundary condition, the system is closed. In this paper, the fluid and water is assume to be the incompressible viscous flow and obey the Eq. (2).

2.2. Distributed Lagrange-Multiplier (DLM) formulation

In Patankar's work [17, 23], the rigid body occupying the domain Ω_r, which can be considered as a fluid and obey the following governing equation

$$\rho\left[\frac{\partial \boldsymbol{u}}{\partial t}+(\boldsymbol{\nabla u})\boldsymbol{u}\right]=\boldsymbol{\nabla}\cdot\boldsymbol{\sigma}+\rho\boldsymbol{g} \qquad \text{in } \Omega_r \tag{3a}$$

$$\boldsymbol{D}[\boldsymbol{u}]=\boldsymbol{0} \qquad \text{in } \Omega_r \tag{3b}$$

The stress tensor is modelled by

$$\boldsymbol{\sigma}=-p\boldsymbol{I}+\boldsymbol{D}[\boldsymbol{\lambda}], \tag{4}$$

where $\boldsymbol{I}$ is the identity tensor, p is the pressure and $\boldsymbol{\lambda}$ is the Lagrange multiplier due to the rigidity constraint Eq. (3b). Some physical interpretations of the formulation has been given through the point of view of a viscoelastic fluid [5] or a elastic solid [24].

2.3. Modified DLM formulation for rigid body dynamics

In this work, two modification will be made on formulation. First, the pressure is separated from the Cauchy stress tensor to be consistence with the Navier-Stokes equations. From Eq. (3b), we have $\frac{\partial u}{\partial x}=0$; $\frac{\partial v}{\partial y}=0$; $\frac{\partial w}{\partial z}=0$, and so $\boldsymbol{\nabla}\cdot\boldsymbol{u}=0$. Because the rigid constraint is more strict than the incompressibility constraint. Substitute Eq. (4) into Eq. (3a), the linear momentum Eq. (3a) becomes

$$\rho\left[\frac{\partial \boldsymbol{u}}{\partial t}+(\boldsymbol{\nabla u})\boldsymbol{u}\right]=-\boldsymbol{\nabla}p+\boldsymbol{\nabla}\cdot\boldsymbol{D}[\boldsymbol{\lambda}]+\rho\boldsymbol{g} \tag{5}$$

In addition, it is proved in Lemma 1 that if $\boldsymbol{D}[\boldsymbol{u}]=\boldsymbol{0}$ is given, there will be

$$\boldsymbol{u}_r=\boldsymbol{U}+\boldsymbol{\omega}\times\boldsymbol{x} \tag{6}$$

On this basis, one can define a rigid velocity field projection operator P as

$$\boldsymbol{u}_r - \mathsf{P}(\boldsymbol{u}) = \boldsymbol{0}. \tag{7}$$

which projects any arbitrary velocity field $\boldsymbol{u}$ into a rigid velocity field $\boldsymbol{u}_r$. The rigid velocity constraint (4) are replaced by Eq. (7). Substitution of the above new kinematic constrain Eq. (7) into the spatial derivative of the linear momentum equation (5), yieldings

$$\rho\left[\left(\frac{\partial \mathsf{P}(\boldsymbol{u})}{\partial t}\right) + (\boldsymbol{\nabla}\mathsf{P}(\boldsymbol{u}))\mathsf{P}(\boldsymbol{u})\right] = -\boldsymbol{\nabla}p + \boldsymbol{\nabla}\cdot\boldsymbol{D}[\boldsymbol{\lambda}] + \rho\boldsymbol{g}. \tag{8}$$

The overall governing equation for a rigid body dynamics, which is comparable with the Navier-Stokes Eqs. (2)

$$\rho\left[\frac{\partial \boldsymbol{u}}{\partial t} + (\boldsymbol{\nabla}\boldsymbol{u})\boldsymbol{u}\right] = -\boldsymbol{\nabla}p + \boldsymbol{\nabla}\cdot\boldsymbol{D}[\boldsymbol{\lambda}] + \rho\boldsymbol{g} \tag{9a}$$

$$\boldsymbol{\nabla}\cdot\boldsymbol{u} = 0 \tag{9b}$$

$$\boldsymbol{\nabla}\cdot\boldsymbol{D}[\boldsymbol{\lambda}] = \rho\left[\left(\frac{\partial \mathsf{P}(\boldsymbol{u})}{\partial t}\right) + (\boldsymbol{\nabla}\mathsf{P}(\boldsymbol{u}))\mathsf{P}(\boldsymbol{u})\right] + \boldsymbol{\nabla}p - \rho\boldsymbol{g} \tag{9c}$$

Above Eq. (9) is the strong form of the governing equation for the rigid body dynamics. Compared with the N-S Eq. (2), the only difference is the evaluation of $\boldsymbol{\nabla}\cdot\boldsymbol{D}[\boldsymbol{\lambda}]$. The rigidity force is clearly stated on the continuum level and it will inspire the 'one-fluid' formulation for the wave interaction with rigid body proposed in this work.

It is worth noting that substituting the $\boldsymbol{u} = \boldsymbol{u}_c + \boldsymbol{\omega}\times\boldsymbol{x}$ into the linear momentum conservation equation Eq. (9a) and its corresponding angular momentum equation will recover the Newton-Euler formulation Eq. (2a), which is shown in Lemma 2. On the continuum level, the angular momentum equation is automatically satisfied because of the symmetric of $\boldsymbol{D}[\boldsymbol{\lambda}]$.

2.4. Fluid-structure interaction: one-fluid formulation

In general, the continuum can contain internal interfaces separating different subdomains or phases (i.e. fluid-fluid, solid-fluid, fluid-solid). In this case, suitable jump conditions can be introduced on very interface. In the case of immersed methodologies, the explicit use of the jump conditions is avoided by means of a 'smooth regularisation' of the interface. Followed immersed methodologies, with the new formulation Eq. (9) for the rigid body dynamics, the conservation equation for the linear momentum for three-phase system can be expressed in a single equation in the whole domain $\Omega = \Omega_a \cup \Omega_w \cup \Omega_r$ (in the absence of surface tension), where the subscript a, w, r denotes the air, water and rigid body phases, respectively.

$$\begin{aligned}\rho\left[\frac{\partial \boldsymbol{u}}{\partial t} + (\boldsymbol{\nabla}\boldsymbol{u})\boldsymbol{u}\right] &= -\boldsymbol{\nabla}p + \boldsymbol{f} + \rho\boldsymbol{g}\\ \boldsymbol{\nabla}\cdot\boldsymbol{u} &= 0\end{aligned}. \tag{10}$$

where $\rho = \rho_r H_r + \rho_w H_w + \rho_a H_a$ and $\boldsymbol{f} = \boldsymbol{\nabla} \cdot 2\mu_a \boldsymbol{D}(\boldsymbol{u}) H_a + \boldsymbol{\nabla} \cdot 2\mu_w \boldsymbol{D}(\boldsymbol{u}) H_w + f_r H_r$. In these expressions, H_a is the generalised Heaviside function for a phase a, which is defined as

$$H_a(\boldsymbol{x}) = \begin{cases} 1 & \text{if} \quad \boldsymbol{x} \in \Omega_a \\ 0 & \text{if} \quad \boldsymbol{x} \notin \Omega_a \end{cases} . \tag{11}$$

In the Eq. (10), the force $\boldsymbol{f}$ is defined on each phase

$$\boldsymbol{f} = \begin{cases} \boldsymbol{\nabla} \cdot 2\mu_a \boldsymbol{D}(\boldsymbol{u}) & \text{air} \\ \boldsymbol{\nabla} \cdot 2\mu_w \boldsymbol{D}(\boldsymbol{u}) & \text{water} \\ \rho \left[\left(\frac{\partial \mathsf{P}(\boldsymbol{u})}{\partial t} \right) + (\boldsymbol{\nabla} \mathsf{P}(\boldsymbol{u})) \mathsf{P}(\boldsymbol{u}) \right] + \boldsymbol{\nabla} p - \rho \boldsymbol{g} & \text{rigid} \end{cases} . \tag{12}$$

This approach is classically known as the 'one-fluid' formulation in the context of multiphase flows [25] and is pursued in this paper. The formulation is named 'one-fluid' because the governing Eq. (10) is similar to those of the single phase N-S Eq. (2). The above Eq. (10) is exactly rewrite the three-phases equations for the whole domain and satisfy the non-slip boundary on the interface without resorting to the jump condition [1]. The solution can change discontinuously across the interface, which is the reason for introducing the generalised Heaviside function or sometimes called the indicator function H. Until now, there is no numerical approximation or Lagrange particle/meshes introduced in the formulation.

3. Geometric problem: Heaviside function for three phases

The 'one-fluid' formulation relies on the correct identification of the interface between the different phases of the continuum so as to evaluate correctly the Heaviside function. The movement of the Heaviside function by external velocity is a geometric problem. The problem can be written as:

$$\frac{DH_i}{Dt} = 0 \tag{13}$$

In this work, we will rely on the existing work for the Level Set method for two phase flows, and adding the rigid Heaviside on it. The basic Level Set Method was developed by Osher and Sethian [26] and further developed for multiphase flow simulations [27]. The function ϕ is defined as a signed distance function, and the contour $\phi = 0$ defines the interface.

$$\Gamma_t = \{\boldsymbol{x} \in \mathbb{R}^2 \mid \phi(\boldsymbol{x}, t) = 0\}, \tag{14}$$

where $\phi(\boldsymbol{x}) = \text{sgn}(\boldsymbol{x}) \cdot \text{ dist}(\boldsymbol{x}, \Gamma_t)$ and $\text{dist}(\boldsymbol{x}, \Gamma_t)$ denotes the distance to Γ_t, and sgn assumes to take positive values inside and the negative value outside.

$$\text{sgn}(\boldsymbol{x}) = \begin{cases} -1 & \textit{if} \quad \boldsymbol{x} \in \Omega \\ 1 & \textit{if} \quad \boldsymbol{x} \notin \Omega \end{cases} , \tag{15}$$

[1] The kinematic and dynamic B.C. has been illustrated in Lemma (3).

The follow steps will explain how to describe the interfaces by three Heaviside function.

- Ignoring the rigid body, a Level Set function ϕ is introduced to identify the interface between the air and water, similar to the two-phase problem.
- A rigid Heaviside function H_r is introduced to identify the rigid body region.
- The rigid, air and fluid domain occupied in $\Omega_{rigid}, \Omega_{air}, \Omega_{water}$ can be defined as

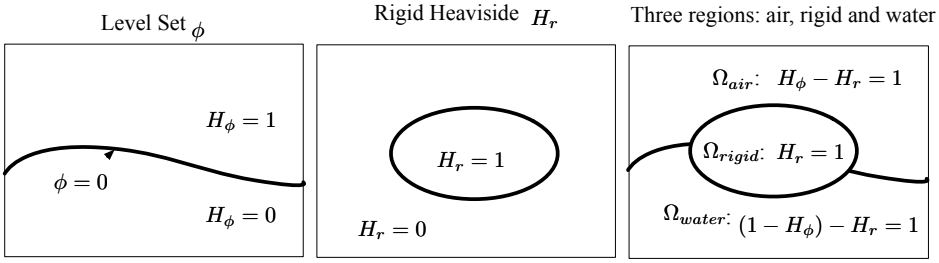

Figure 1: Illustration of the representation of three phases using two Heaviside function

$$\begin{aligned} \Omega_{rigid} &= \{\boldsymbol{x} \in \mathbb{R}^{2,3} \mid H_r(\boldsymbol{x}, t) = 1\} \\ \Omega_{water} &= \{\boldsymbol{x} \in \mathbb{R}^{2,3} \mid (H_\phi(\boldsymbol{x}, t) - H_r(\boldsymbol{x}, t)) = 1\} \\ \Omega_{air} &= \{\boldsymbol{x} \in \mathbb{R}^{2,3} \mid (1 - H_\phi(\boldsymbol{x}, t) - H_r(\boldsymbol{x}, t) = 1\} \end{aligned} \tag{16}$$

as shown in Fig. 1.

Once the Heaviside function has been constructed, the various material properties can be assigned. The Heaviside function should be smeared out, so the corresponding density and viscosity field are smooth on the interface region. In the following, we will explain how to calculate the smoothed Heaviside functions.

3.1. Smoothed fluid Heaviside

3.1.1. Construction

The evolution of phase indicator function H follows naturally as $H_a(\boldsymbol{x}, t) = H(\phi(\boldsymbol{x}, t))$. Following the work of Sussman [27], an approximation of a Heaviside function H can be calculated as

$$H(\boldsymbol{x}) = \begin{cases} \frac{1}{2}(1 + \phi/\epsilon + \sin(\pi\phi/\epsilon)/\pi) & if \quad |\phi/\epsilon| \leq 1 \\ 0 & if \quad \phi/\epsilon < -1 \\ 1 & if \quad \phi/\epsilon > 1 \end{cases}, \tag{17}$$

where ϵ is a parameter that represents the smearing bandwidth. Thus, the approximation of the Heaviside function changes from zero to one over the smearing interface, describing a smooth transition zone from one phase to the next.

3.1.2. Convection

The evolution equation of an interface moving in a medium with velocity $\boldsymbol{u}$, is defined in a Eulerian setting in non-conservative form as

$$\frac{\partial \phi_f(\boldsymbol{x},t)}{\partial t} + \boldsymbol{u}(\boldsymbol{x},t)\cdot\boldsymbol{\nabla}\phi_f(\boldsymbol{x},t) = 0. \tag{18}$$

This equation can be solved by the standard discretisation techniques and followed with a reinitialisation procedure [27] and narrow banded Level Set implementation.

3.2. Smoothed rigid Heaviside

3.2.1. Construction

The convolution procedure is introduced to prescribe an arbitrary Heaviside function in the initial time $t = 0$.

Step 1: Given a Cartesian mesh, we can assign values 1 into the polygon which describe the rigid body, which is non-smoothed discretised Heaviside function H_r, see Fig. 2 (a).

Step 2: Select a smoothed approximation of the Dirac Delta function $\hat{\delta}(\boldsymbol{x})$, see Fig. 2 (b). Numerous Dirac delta function are available in the literature, ranging from Peskin's work [10, 28, 29] to high order smooth function on the immersed boundary community to reduce the high frequency oscillation. Given the arrangement of the structured fluid mesh, a tensor product approximation to the delta distribution has been considered

$$\hat{\delta}(\boldsymbol{x}) = \prod_{i=1}^{i=n} \delta^1_{\Delta x_i}(x_i) \tag{19}$$

where Δx_i is the mesh spacing in the i-th coordinate direction, n is the number of space dimensions and the one-dimensional approximation δ^1_h has been chosen as

$$\delta^1_h(x) = \frac{1}{h}\Psi\left(\frac{x}{h}\right), \tag{20}$$

where Ψ is a continuous function which can be given by any of the possible formulas below[10, 28, 30, 31, 32]. In the particle based formulations, high order kernels is designed to reduce the numerical oscillations. In this method, the kernel is only used for smoothing in the first time step.

Step 3: Convolution of the non-smoothed Heaviside function with a smooth Dirac Delta function to smoothed Heaviside, see Fig. 2 (c).

$$\hat{H}_r = H_r(\boldsymbol{x}) * \hat{\delta}(\boldsymbol{x}) \tag{21}$$

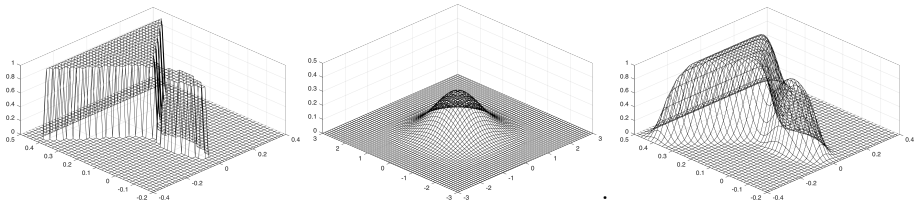

(a) Step 1: Non-smoothed Heaviside function (b) Step 2: Smoothing kernels (c) Step 3: Smoothed Heaviside function after Convolution

Figure 2: Examples of initialisation of a ship section shaped Heaviside function through convolution.

3.2.2. Convection

It is possible to solve the Heaviside convection equation similar to the Volume of Fluid/Level Set method. But in general it is very difficult for the Eulerian methods to preserve the shape of Heaviside during the convection. Instead, a rigid mapping is introduced to linked by $\boldsymbol{\Psi} : \Omega \times [0,T] \rightarrow \mathbb{R}^d$ such that $\boldsymbol{x}(t) = \boldsymbol{\Psi}(\boldsymbol{X}, t)$. The inverse mapping can be written as

$$\boldsymbol{X} = \boldsymbol{\Psi}^{-1}(\boldsymbol{x}(t), t) \tag{22}$$

The material coordinates can be tracked by

$$\frac{d\boldsymbol{X}}{dt} = \boldsymbol{u}(\boldsymbol{x}) = \boldsymbol{\omega} \times \boldsymbol{x} + \boldsymbol{U} \tag{23}$$

And the Heaviside for the rigid body are calculated using its material configuration as

$$H_r(\boldsymbol{x}, t) = H_r(\boldsymbol{X}, 0) \tag{24}$$

The above mapping is calculated via an interpolation scheme. In the section of numerical examples, we will discuss the effect of using three interpolation scheme, C^0 (bilinear), C^1 (bicubic) and C^2 (cubic spline) continuity interpolation.

Following is the set of balance equations that model the wave-rigid body interaction problem

$$\rho\left[\frac{\partial \boldsymbol{u}}{\partial t} + (\boldsymbol{\nabla}\boldsymbol{u})\boldsymbol{u}\right] + \boldsymbol{\nabla}p - \boldsymbol{f} - \rho\boldsymbol{g} = \boldsymbol{0} \qquad \text{in } \Omega \times [0,T] \tag{25a}$$

$$\boldsymbol{f} = \begin{cases} \boldsymbol{\nabla} \cdot 2\mu_a \boldsymbol{D}(\boldsymbol{u}) \\ \boldsymbol{\nabla} \cdot 2\mu_w \boldsymbol{D}(\boldsymbol{u}) \\ \rho\left[\left(\frac{\partial \mathsf{P}(\boldsymbol{u})}{\partial t}\right) + (\boldsymbol{\nabla}\mathsf{P}(\boldsymbol{u}))\mathsf{P}(\boldsymbol{u})\right] + \boldsymbol{\nabla}p - \rho\boldsymbol{g} \end{cases} \qquad \text{in } \Omega \times [0,T] \tag{25b}$$

$$\frac{\partial \phi_f}{\partial t} + \boldsymbol{u} \cdot \boldsymbol{\nabla}\phi_f = 0 \qquad \text{in } \Omega \times [0,T] \tag{25c}$$

$$H_r(\boldsymbol{x}, t) = H_r(\boldsymbol{X}, 0) \qquad \text{in } \Omega \times [0,T] \tag{25d}$$

4. Numerical techniques

In this section, we will discuss the details of the numerical discretisation of the proposed one-fluid formulation for the wave and rigid floating body interaction problem. An efficient low order finite volume scheme set in a Cartesian staggered grid is chosen for the spatial discretisation. The rigidity forces and a new least square projection method will be discussed in details.

4.1. Fluid solver

A two dimensional Cartesian discretisation of the incompressible flow is adopted in conjunction with a staggered second order finite volume approach. A semi-implicit scheme is used for advancement in time and the second-order Adams-Bashforth for the convection term. The algorithm is written as follows:

$$\rho \frac{\boldsymbol{u}^* - \boldsymbol{u}^n}{\Delta t} = RHS^n + \boldsymbol{f}^n \tag{26a}$$

$$\boldsymbol{\nabla} \cdot \left(\frac{\boldsymbol{\nabla} p}{\rho} \right) = - \frac{\boldsymbol{\nabla} \cdot \boldsymbol{u}^*}{\Delta t} \tag{26b}$$

$$\boldsymbol{u}^{n+1} = \boldsymbol{u}^n - \frac{\Delta t}{\rho} \boldsymbol{\nabla} p \tag{26c}$$

where superscript n denotes time step, $\boldsymbol{u}^*$ are the intermediate velocity vectors and $RHS^n = -\rho(\boldsymbol{\nabla u})\boldsymbol{u} + \rho \boldsymbol{g}$. The non-constant diffusion equation is solved using HYPRE library [33]. In the water and air phases, the viscous term $\boldsymbol{f}$ is evaluated by the second order spatial derivatives.

4.2. Rigidity force

Because the scheme Eq. (7) is implicit, applying the rigid constraint is not as straightforward as in the viscous term. To approximately solve the coupled system of equations, we use the $\mathsf{P}(\boldsymbol{u}^n) = \boldsymbol{u}^n$

$$\begin{aligned} \boldsymbol{f}^n &= \rho \left[\frac{\partial \mathsf{P}(\boldsymbol{u}^n)}{\partial t} + (\boldsymbol{\nabla} \mathsf{P}(\boldsymbol{u}^n)) \mathsf{P}(\boldsymbol{u}^n) \right] + \boldsymbol{\nabla} p - \rho \boldsymbol{g} \\ &= \rho \left[\frac{\mathsf{P}(\boldsymbol{u}^{n+1}) - \boldsymbol{u}^n}{\Delta t} + (\boldsymbol{\nabla} \boldsymbol{u}^n) \boldsymbol{u}^n \right] + \boldsymbol{\nabla} p - \rho \boldsymbol{g} \\ &= \rho \left[\frac{\mathsf{P}(\boldsymbol{u}^{n+1}) - \boldsymbol{u}^n}{\Delta t} \right] - RHS^n \end{aligned} \tag{27}$$

- On the proposed semi-discretised form, the scheme is the very similar to the formulation proposed by Patankar. However, the rigid body velocity field is achieved from a kinematics point of view.
- If the $\mathsf{P}(\boldsymbol{u}_{k+1}^{n+1})$ is given by a prescribed motion, the method is exactly a direct forcing method.

4.3. Least square for rigid body motion

For a general motion problem, the projection $\mathsf{P}(\boldsymbol{u})$ is to find $\boldsymbol{U}$ and $\boldsymbol{\omega}$, so that $\mathsf{P}(\boldsymbol{u}) = \boldsymbol{\omega} \times \boldsymbol{x} + \boldsymbol{U}$. This will lead to a least square problem in the Ω_r, so that

$$\text{minimise } ||\mathsf{P}(\boldsymbol{u}) - \boldsymbol{u}||^2 \;\; \textit{or} \;\; \text{minimise } ||\boldsymbol{\omega} \times \boldsymbol{x} + \boldsymbol{U} - \boldsymbol{u}||^2$$

- $\boldsymbol{\omega}$ and $\boldsymbol{U}$ is the variable (to be chosen/found)
- $||\boldsymbol{\omega} \times \boldsymbol{x} + \boldsymbol{U} - \boldsymbol{u}||^2$ is the objective function
- $\hat{\boldsymbol{\omega}}$ and $\hat{\boldsymbol{U}}$ is a solution of this problem if $||\hat{\boldsymbol{\omega}} \times \boldsymbol{x} + \hat{\boldsymbol{U}} - \boldsymbol{u}||^2 < ||\boldsymbol{\omega} \times \boldsymbol{x} + \boldsymbol{U} - \boldsymbol{u}||^2$ holds for any $\boldsymbol{\omega}$ and $\boldsymbol{U}$

For the problem of allowed translational motion or only allowed rotation, the objective function is simplified to $||\boldsymbol{U} - \boldsymbol{u}||^2$ or $||\boldsymbol{\omega} \times (\boldsymbol{x} - \boldsymbol{x}_c) - \boldsymbol{u}||^2$ respectively, where $\boldsymbol{x}_c$ is the rotation centre already known. Because of the smoothed Heaviside function, there is a region mixed with fluid and rigid in $0 < H(\boldsymbol{x}) < 1$. In practise, the weighted linear least squares problem is solved, where the rigid Heaviside function $H_r(\boldsymbol{x})$ associated with spatial coordinates $\boldsymbol{x}$ act as weights.

The proposed approach above permits the simulation of several rigid motions including the allowed rotation, allowed translation or the free rigid body motion in a same algorithm. It can be observed that different rigid body motions lead to different construction of the objective function.

4.4. Algorithm

For completeness, the flowchart of overall algorithm employed in this paper is included to illustrate the various steps of the methodology presented here.

Algorithm One Fluid Formulation for Wave and Rigid body interaction

- Initialise the fluid velocity $\boldsymbol{u}_0$, Level Set $\boldsymbol{\phi}$ and Heaviside function $\boldsymbol{H}$ though convolution.
- Loop over time

1 Compute an intermediate velocity field $\boldsymbol{u}^*$ by advancing the 'one-fluid' momentum equation without considering the viscous and rigidity force

$$\rho(\frac{\boldsymbol{u}^* - \boldsymbol{u}^n}{\Delta t}) = RHS^n.$$

where $RHS^n = -\rho(\boldsymbol{\nabla} \boldsymbol{u}^n)\boldsymbol{u}^n + \rho \boldsymbol{g}$

2 Evaluate the rigidity force $\boldsymbol{f}^n$ in Ω_r.

1. **Linear least square:** Find the rigid velocity field $\mathsf{P}(\boldsymbol{u}^*)$ by minimising $||\mathsf{P}(\boldsymbol{u}^*) - \boldsymbol{u}^*||^2$.
2. **Updating** the rigid body force as

$$\boldsymbol{f}^n = \rho \left[\frac{\mathsf{P}(\boldsymbol{u}^*) - \boldsymbol{u}^n}{\Delta t} \right] - RHS^n$$

3 Evaluate the viscous term $\boldsymbol{f}^n = \mu \boldsymbol{\nabla} \cdot 2\mu \boldsymbol{D}(\boldsymbol{u}_n)$.

4 Compute an intermediate velocity field $\boldsymbol{u}^{**}$ by advancing the 'one-fluid' momentum equation considering the viscous and rigidity force

$$\rho(\frac{\boldsymbol{u}^{**} - \boldsymbol{u}^n}{\Delta t}) = RHS^n + \boldsymbol{f}^n.$$

5 Compute the pressure to satisfy the incompressible constraint with Neumann boundary condition

$$\boldsymbol{\nabla} \cdot \left(\frac{\boldsymbol{\nabla} p^n}{\rho} \right) = -\frac{\boldsymbol{\nabla} \cdot \boldsymbol{u}^{**}}{\Delta t}.$$

6 Apply velocity correction

$$\boldsymbol{u}^{n+1} = \boldsymbol{u}^{**} - \frac{\Delta t}{\rho} \boldsymbol{\nabla} p^n.$$

7 Convecting Level Sets and reinitilisation.

8 Convecting rigid Heaviside function via high order interpolation

9 Update velocity $\boldsymbol{u}^{n+1}$, density ρ^{n+1} to the next time step.

5. Numerical examples

The proposed formulation is applied to simulate the complex FSI problem involving the free surface. Four test cases, prescribed motion, free motion, allowed rotation and allowed translation are conducted to demonstrate the accuracy and applicability of the proposed method.

5.1. Water entry of a horizontal circular cylinder

With a prescribed rigid body motion, the proposed method becomes a direct forcing method. In this example ,we will study a cylinder impacting on water with bodies undergoing a prescribed velocity. It has been numerically studied in [34, 35, 36]. The same dimensionless parameters in [35, 36] will be used: a circular cylinder of radius $R = 1$ is placed in air and the distance of its centre to the air-water interface is $H = 1.25$. The gravity's acceleration is set to be $\boldsymbol{g} = (0, -1)^T$ and the cylinder is given a constant downward velocity $u_y = -1$ at the $t = 0$ with t the time in the calculation. The computational domain is set to be $\Omega = [40R \times 24R]$. The air dynamic viscosity is $\mu_a = 1.0 \times 10^{-5}$ with density $\rho_a = 1$. The water dynamic viscosity is $\mu_w = 1.0 \times 10^{-3}$ with density $\rho_a = 1 \times 10^{-3}$. The geometric description of the example is shown in Fig. 3. In our method, we need to specify the rigid body density, which is chosen to be $\rho_r = 1$. Although this numerical example does not involve in the rigid body dynamics, it will demonstrate some important features of the algorithm, capable of capturing surface and the unphysical pressure oscillation. Four set of meshes is used for the simulation, where $dx = 0.1R \times (\frac{1}{2})^i$, where $i = 0, 1, 2, 3$.

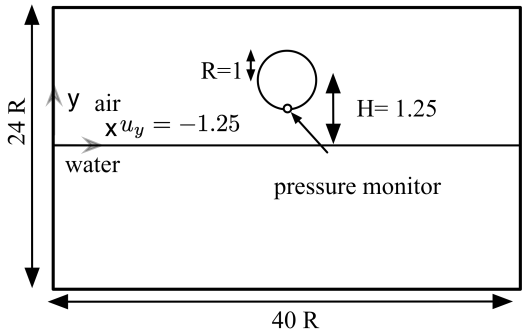

Figure 3: Schematic description for the cylinder water entry problem

Fig. 4 shows the free surface pattern along with the mesh refinement at time $t = 1$. A wave that grows and steepens up depending on the grid resolution.

Fig. 5 shows the effect of using different interpolation scheme (bilinear, bicubic and cubic spline) for the movement of the rigid Heaviside function. The pressure monitoring point is chosen as the bottom of the circular cylinder. Using higher order spline, which is C^2 continuity, will reduce the numerical ossification significantly. So we will use the C^2 for the rest of the numerical

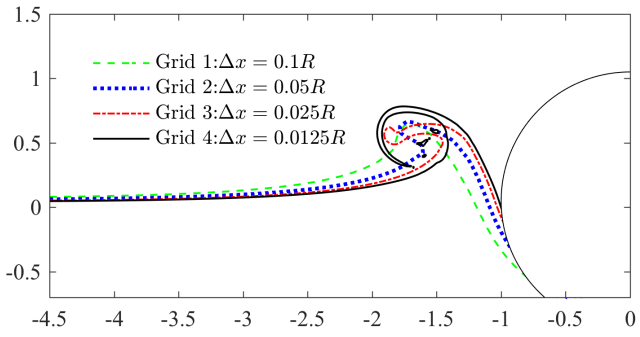

Figure 4: Water entry of a horizontal circular cylinder moving with prescribed velocity. Influence of the grid refinement on the free surface position at time $t = 0.8$.

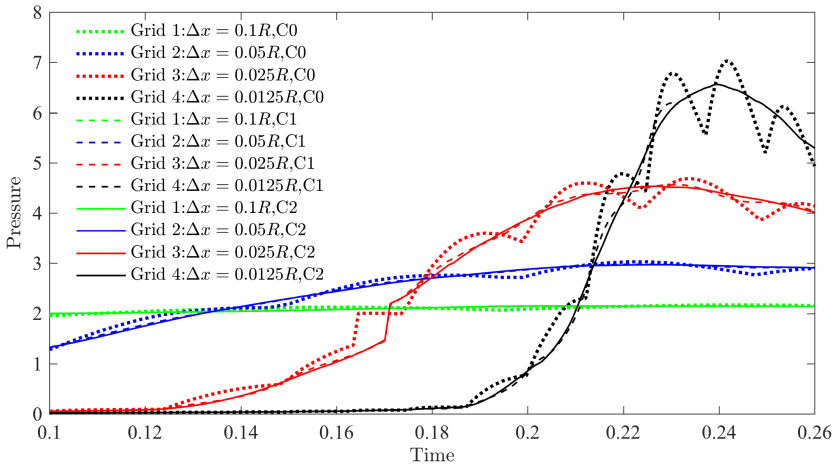

Figure 5: The evolution of pressure at the monitor point with time, by C^0 (bilinear), C^1 (bicubic) and C^2 (cubic spline) continuity interpolation scheme and four set of meshes.

simulation. In the immersed boundary community, some authors designed the high order kernels to reduce the oscillation. We have also tested using the high order kernels for the initialisation of the smoothed Heaviside function, but it does not effect the results. Because the Heaviside is constructed by interpolation rather than integration of the particles.

We can also observe in Fig. 5 that the coarse mesh can not predict the pressure peak, even the free surface profiles is captured. We will discuss about the peak pressure in details in the last numerical example.

A series of snapshots are shown in Fig. 6. For the entry problem impacts the air-water interface, two jets are generated along the left and right side of the cylinder. Several vortices shedding from the shear layers along the surface of the cylinder interact with the air-water interface. The results are very similar to [35, 36].

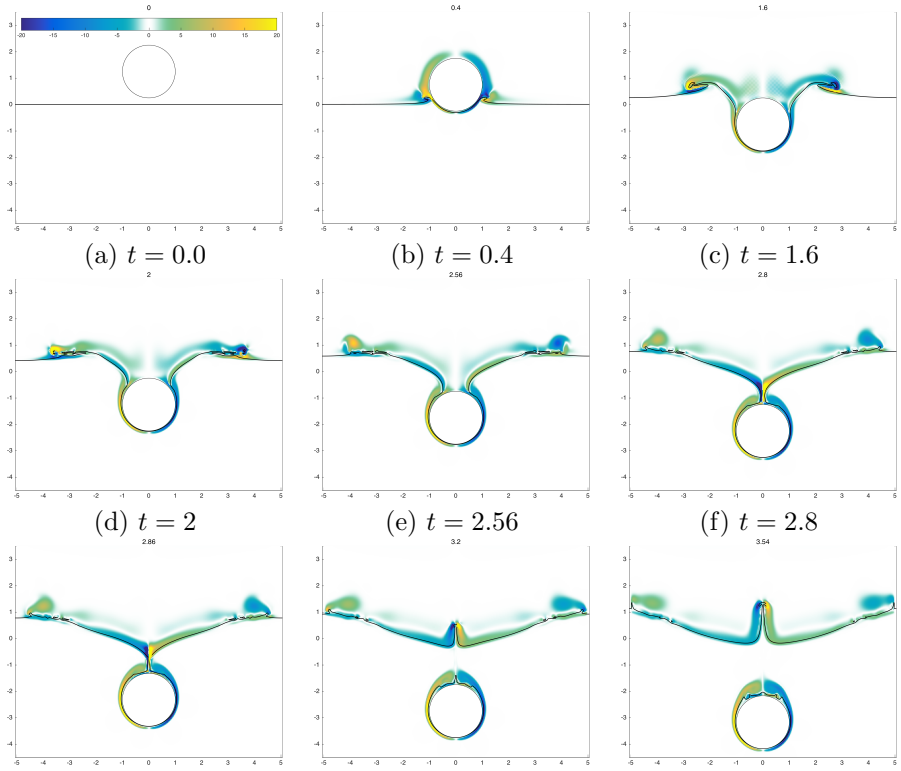

(a) $t = 0.0$ (b) $t = 0.4$ (c) $t = 1.6$

(d) $t = 2$ (e) $t = 2.56$ (f) $t = 2.8$

(g) $t = 2.86$ (h) $t = 3.2$ (i) $t = 3.54$

Figure 6: Water impact problem: the air-water interface position (solid black line) and vorticity contours ($-20 < \omega < 20$), $g = -1$, constant velocity $\boldsymbol{u}_y = -1$, mesh grid 400×240, the radius of rigid cylinder $R = 1$.

5.2. Free heave decay test of a circular cylinder

This example shows the wave interaction with rigid body algorithm, where the rigid body is driven by the its gravity, buoyancy and the viscous effect from the air and water. The experimental result has been investigated by Ito [37]. A horizontal circular cylinder of a diameter $D = 0.1524$ m and density $\rho = 500$ kg/m^3 is partially submerged with its centre positioned 0.0254 m above the free surface rectangular channel at time $t = 0$, and then release. The cylinder will oscillate and a system of waves will be generated and propagate away from the cylinder. Due to the viscous effect and the generated wave, the amplitude position of the cylinder will decay very quickly. To analysis the accuracy and

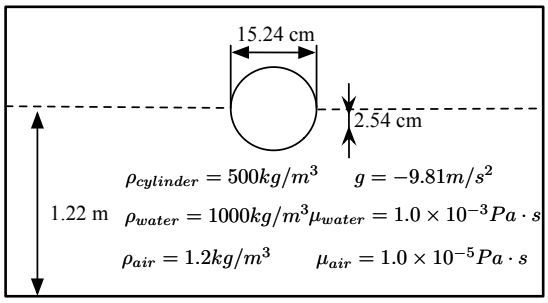

Figure 7: Schematic description of the cylinder configuration study by [37].

Table 1: Description of four grids employed in the free heave decay test of a circular cylinder

n	Δx (m)	grid size
1	1×10^{-2}	180×20
2	5×10^{-3}	360×40
3	2.5×10^{-3}	720×80
4	1.25×10^{-3}	1440×160

convergence and the algorithm, four uniform meshes have been employed as follows : grid 1 with 180×20; grid 2 with 360×40; grid 3 with 720×80 and grid 4 with 1440×160 grid in the horizontal and vertical direction. Fig. 8 shows the normalised position of the cylinder evolution with time. It can be seen that the proposed method under the finest mesh is able to accurately predict the frequency of the oscillation as well as its amplitude.

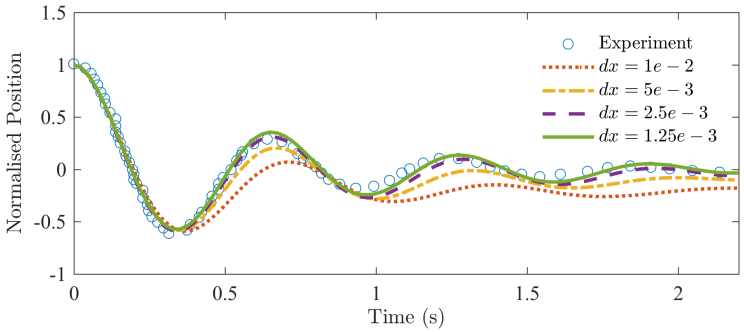

Figure 8: Convergence study of free heave decay of a circular cylinder.x axis: time. y axis: Normalised position of the cylinder.

5.3. Free roll decay of a 2-D rectangular barge

The aim of this example is to validate the algorithm under a single degree of rotation. The viscous effect on the roll motion of a rectangular structure has been investigated by [38]. The barge is allowed to rotate freely with respect to a fix point. The numerical studies has been given by immersed boundary method [16]. It is initially placed at an angle of 15 degree as shown in Fig. 9. In contrast with other simulations, we only needs the density of the rigid body rather than the inertia. By using the rectangular inertia equation $I_z = \frac{\rho ab(a^2+b^2)}{12}$[2], the density of the rigid body is $\rho = 856$ kg/m^3, consistent with the inertia $I_z = 0.236$ kg/m^3 measured in the experiment. The gravity's acceleration is set to be $\boldsymbol{g} = (0, -9.8)^T$ m/s^s. Free slip condition is applied at the side walls of the channel. Three uniform meshes have been employed as follows : grid 1 with

Table 2: Description of four grids employed in the free roll decay test of a rectangular barge

n	Δx (m)	grid size
1	6.4×10^{-3}	320×128
2	3.2×10^{-3}	640×256
3	1.6×10^{-3}	1280×512
4	0.8×10^{-3}	2560×1024

320×128; grid 2 with 640×256 and grid 3 with 1280×512 in the horizontal and vertical direction.

Several snapshots on grid 4 shows the position of the barge, free surface and corresponding vorticity contours $-20 < \Omega < 20$. The results shows a good agreement with the experiment in frequency but less damping for the amplitude, which may due to the friction of the experimental appartus [16]. This example

[2]In the formulation, $a = 0.3$ m and $b = 0.1$ m denote the length of the rectangular and width of the rectangular, respectively.

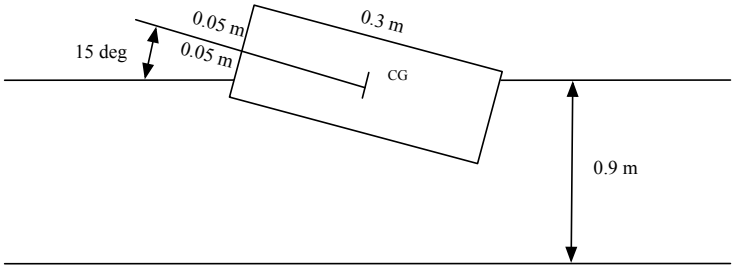

Figure 9: FSI simulation of a roll decay of a rectangular barge. Schematic description of the barge configuration studied by [39].

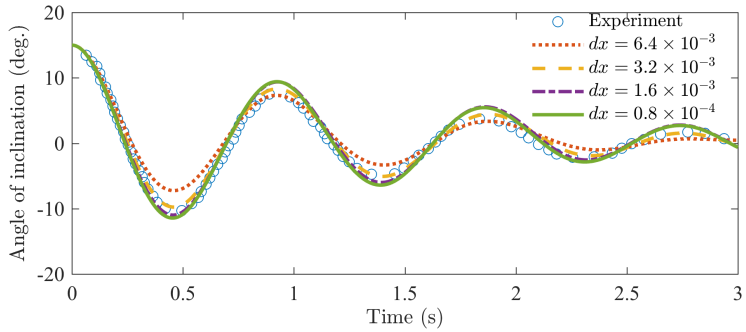

Figure 10: Convergence study of free roll decay of a rectangular barge. Computed angle of inclination of the barge on a series of refined grids. x axis is the time in s and y axis is the angle of inclination in deg.

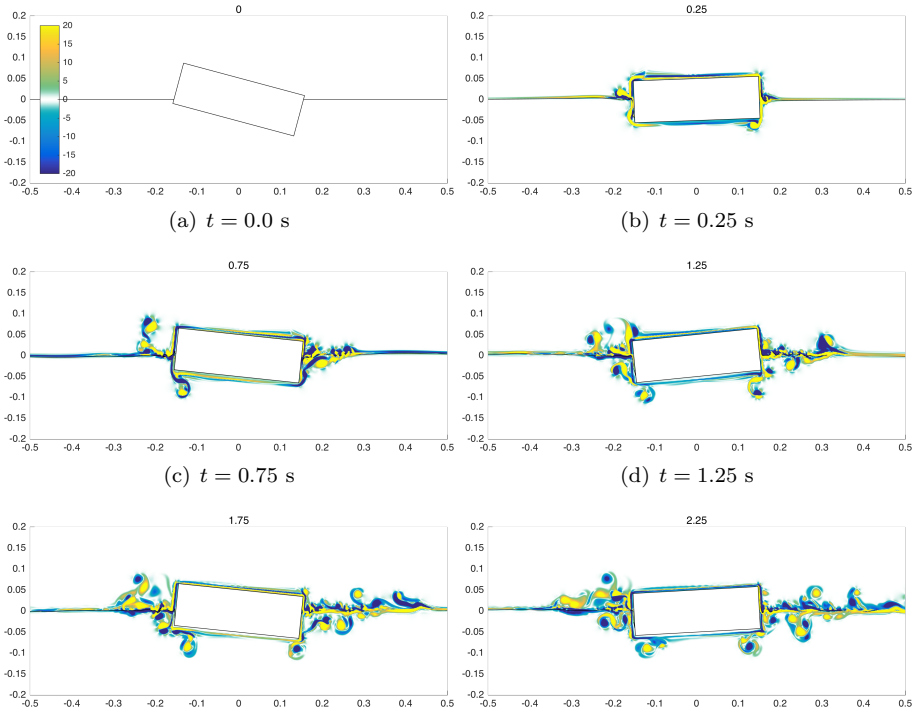

(a) $t = 0.0$ s (b) $t = 0.25$ s

(c) $t = 0.75$ s (d) $t = 1.25$ s

(e) $t = 1.75$ s (f) $t = 2.25$ s

Figure 11: Several snapshots of the position of the barge, free surface and corresponding vorticity contours are shown. The vorticity scale is $-20 < \omega < 20$.

demonstrates the ability of the proposed method for solving the coupled wave and floating rigid body.

5.4. Water impact simulation

This example presents the prediction of impact loads involves the simulation of a two dimensional wedge and ship-section, falling vertically into the free surface. Similar water impact problem investigate the dynamics of the floating body motion [34], free surface profiles and the flow patterns [16], but reported only limited information about the pressure and force. In the context of the ship design, however, the time history of the impact pressure and force is considered to be the most important quantity. Systematic series of experimental impact tests have been performed in WILS JIP (Wave Induced Loads on Ships Joint Industry Project)-III [40] recently. Here we consider three cases in this numerical tests. The geometry and physical property of the experiment is shown in Fig. 12. More details of the experimental setup can be found in [40]. There is a set of pressure sensors and force sensors in the experiment, we only present the one pressure sensor for selected case 1 and one force sensor fir case 2 due to the limitation of space. Other results exhibit similar pattern.

Case 1 is a wedge shape, with dead-rise angle 30 degree and the width of 0.6 m. Initially, the wedge is placed at 0.5 m above the free surface and starts moving under the gravity along the slider. The pressure sensor is placed 0.05 m vertical to the centre of the wedge. The water depth is 1 m, and total weight of the frame, rod and the model is 68.3 kg. In the simulation, we simplify it into a two dimension problem, which is equal to structure density $\rho_s = 1643 \times 10^3$ kg/m^3.

Similarly, the ship section has a weight of 128.54 kg and is equal to structure density $\rho_s = 1074.3 \times 10^3$ kg/m^3. The case 2 and case 3 has the same ship section placed on different height. The ship section width is 0.718 m and height of 0.541 m. In case 2, a ship-section is placed 0.17 m under the water surface, while the ship-section in case 3 is placed under the surface. The force sensor has a section length of 0.05 m and is placed 0.339 m above bottom.

For all simulations, the gravity's acceleration is set to be $\boldsymbol{g} = (0, -9.8)^T$ m/s^s. The air viscosity is $\mu_a = 1.0 \times 10^{-5}$ Pa·s with density $\rho_a = 1.0$ kg/m^3. The water viscosity is $\mu_w = 1.0 \times 10^{-3}$ Pa·s with density $\rho_w = 1000$ kg/m^3.

5.4.1. Water impact case 1, wedge dropping at $h = 0.5$ m.

Five uniform meshes have been employed, illustrated in Table 3. To illustrate the complex flow patterns that develop from the beginning, Fig. 13 shows a series of snapshots of the simulated flow patterns along with the contour fields of the vorticity. The symmetric vortices have been generated behind the wedge can be observed. Fig. 5.4.1 (a) and (b) illustrate the convergence of the wedge velocity under mesh refinement and compared with the experimental data. With the mesh refinement, the acceleration is approximating to the gravity 9.8 m/s^2. It is noticed that the velocity of the wedge agrees well with the experiment for the last three set of meshes. The predication of the velocity or the position does not requires much of the computational power.

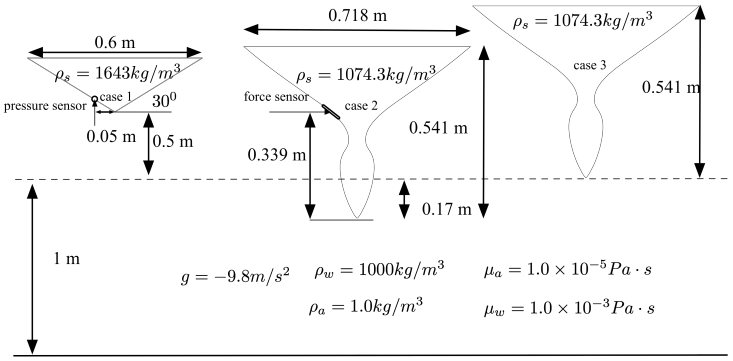

Figure 12: Schematic description of the wedge configuration studied by [40].

Table 3: Description of five grids employed in the water impact problem for case 1.

n	Δx (m)	grid size
1	8×10^{-3}	112×112
2	4×10^{-3}	224×224
3	2×10^{-3}	448×448
4	1×10^{-3}	896×896
5	5×10^{-4}	1792×1792

Due to the large impact that develop on the structure, the prediction of the peak pressure is interested for the engineering purposes. Fig. 5.4.1 (c) shows the time history of the pressure on the location of the pressure sensor, by taking the atmospheric pressure to zero. The pressure oscillation patten similar in Fig. 5 can be observed if using the linear interpolation. All the results shown here uses the cubic spline interpolation to reduce the oscillation. All set of meshes can predict the after peak values very well compared with the experiment. Same conclusion may also be drawn for the case 2 and case 3, as shown in Fig. 16 (b) and Fig. 19 (b). In order to capture the peak pressure, we need a very fine mesh to $dx = 0.5$ mm.

During the numerical simulation, we found that the peak pressure occurs at time $t = 0.33$ s and reaches over 35 kPa. Fig 15 shows the continuous pressure contour plot. The location of the maximum pressure can be observed on the air-water-rigid interface and it moves alongs the edge.

5.4.2. Water impact case 2, ship section dropping at $h = -0.17$ m.

This example illustrates the proposed method is capable of solving a complex rigid geometry, like a ship section. Five uniform meshes have been employed listed in Table 4. Fig. 16 shows a series of snapshots of the simulated flow patterns along with the contour fields of the vorticity, as well as the free surface. Very little air bubbles are entrapped by the ship section.

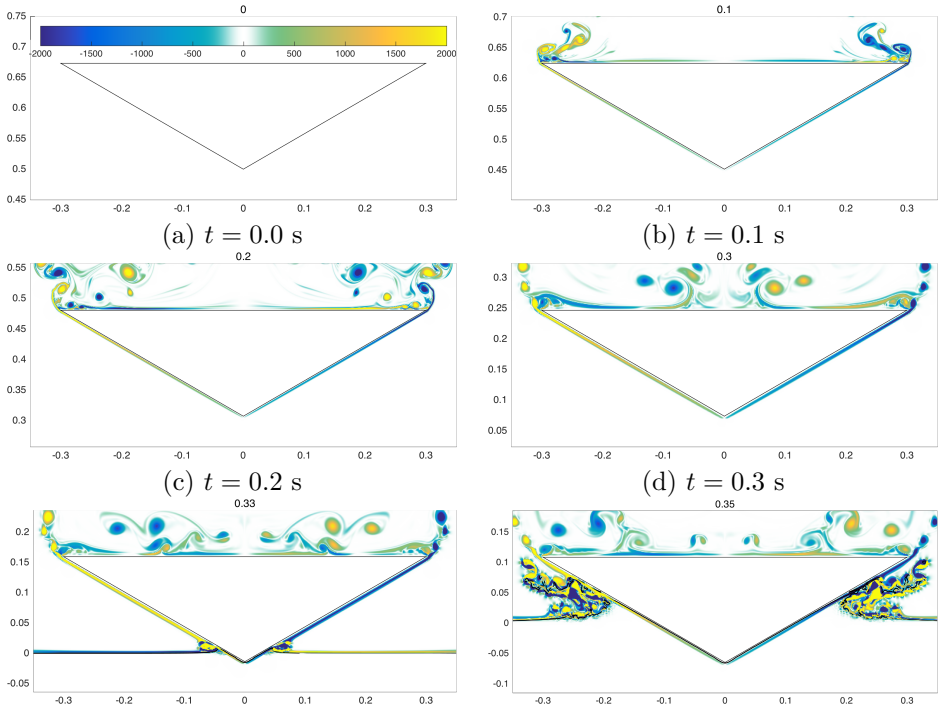

(a) $t = 0.0$ s (b) $t = 0.1$ s (c) $t = 0.2$ s (d) $t = 0.3$ s (e) $t = 0.33$ s (f) $t = 0.35$ s

Figure 13: Water impact problem (case 1): the air-water-rigid interface position (solid black line) and vorticity contours ($-2000 < \omega < 2000$), $dx = 5 \times 10^{-4}$ m.

Table 4: Description of five grids employed in the water impact problem for case 2.

n	Δx (m)	grid size
1	8×10^{-3}	144×120
2	4×10^{-3}	288×240
3	2×10^{-3}	576×480
4	1×10^{-3}	1152×960
5	5×10^{-4}	2304×1920

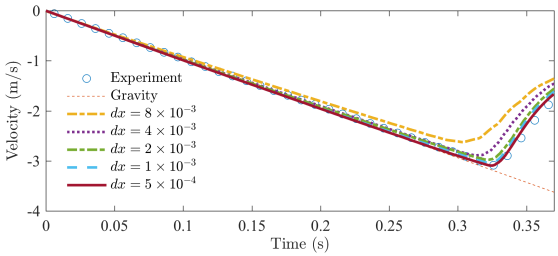

(a) Wedge velocity with mesh refinement

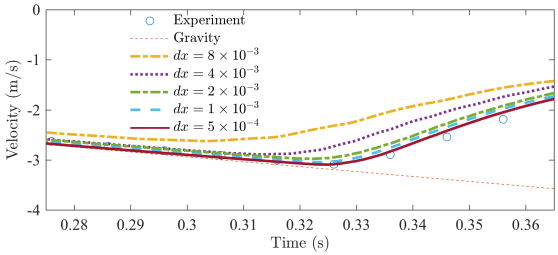

(b) Wedge velocity close view.

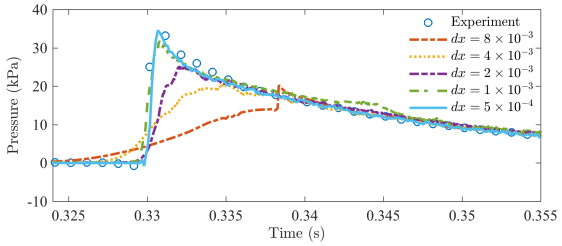

(c) Pressure on the monitoring point.

Figure 14: Water impact problem (case 1): time history of wedge velocity and pressure under mesh refinement, compared with experimental data.

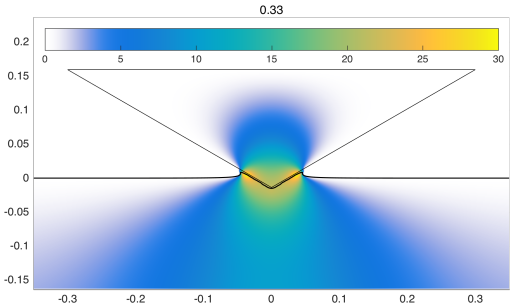

Figure 15: Water impact problem (case 1): pressure distribution (kPa) at time $t = 0.33$ s on the $dx = 5 \times 10^{-4}$ m.

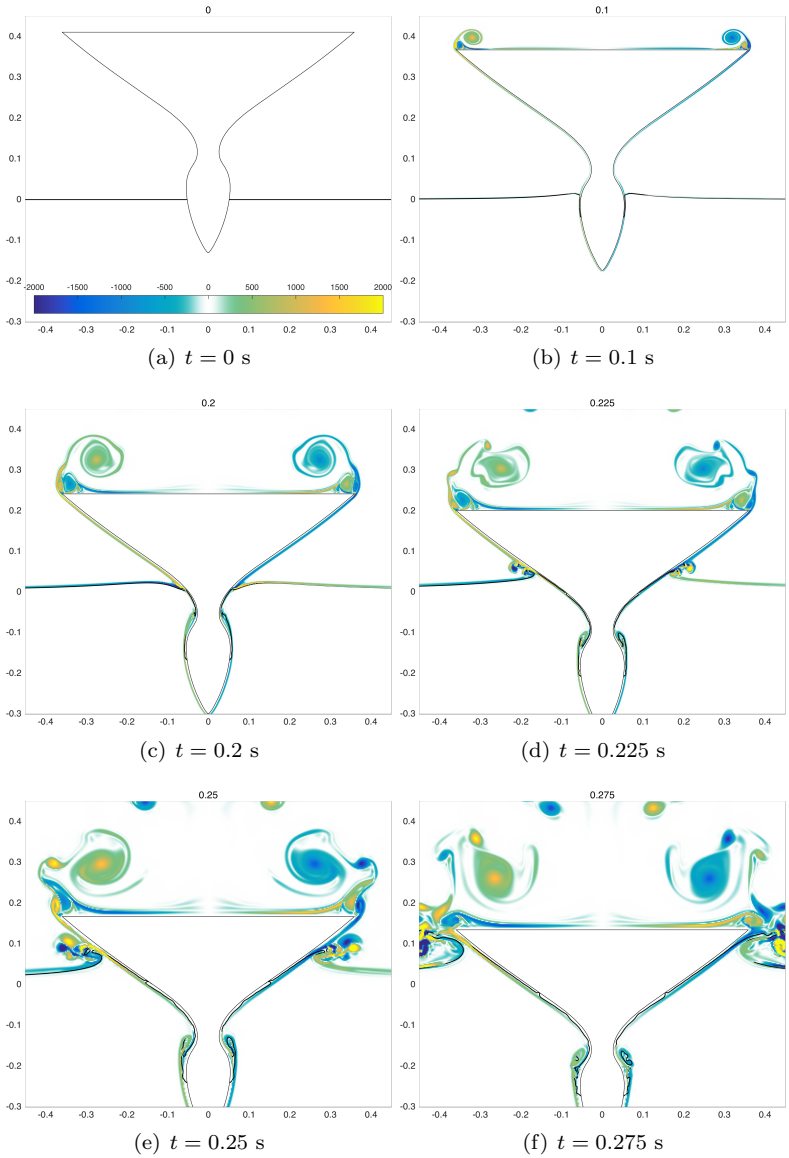

(a) $t = 0$ s (b) $t = 0.1$ s

(c) $t = 0.2$ s (d) $t = 0.225$ s

(e) $t = 0.25$ s (f) $t = 0.275$ s

Figure 16: Water impact problem (case 2): the air-water-rigid interface position (solid black line) and vorticity contours ($-2000 < \omega < 2000$), $dx = 5 \times 10^{-4}$ m.

Fig. 17 shows the time history of the ship section velocity and force on the monitoring section with mesh refinement. The peak force in the finest mesh is larger than the experimental measurement.

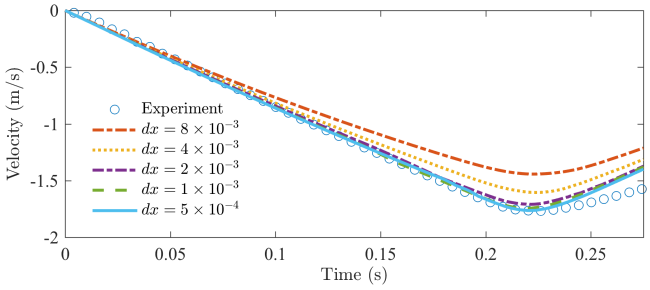

(a) Ship section velocity. x axis is the time in s, y axis is the velocity in m/s.

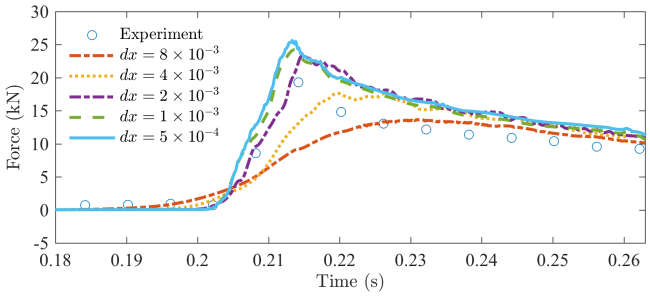

(b) Force on the monitoring region.

Figure 17: Water impact problem (case 2): time history of velocity (a) and force (b) on the monitoring region under mesh refinement, compared with experimental data.

During the numerical simulation, we found that the peak pressure at the monitoring point occurs at time $t = 0.2104$ s and reaches to 13 kPa. Fig. 18 shows the continuous pressure contour plot. The location of the maximum pressure can be observed on the edge. Fig. 22 shows the grid convergence rate of the peak velocity, peak pressure and peak force by taking the finest mesh as the reference. The overall algorithm shows the at least first order grid convergence rate.

5.4.3. Water impact case 3, ship section dropping at $h = 0$ m.

The entrapped air is considered to be an important phenomenon in the ship section dropping test. Case 3 is presented to show the proposed method is capable of capturing the air during the impact. Four uniform meshes have been employed, illustrated in Table 5.

Fig. 19 shows a series of snapshots of the simulated flow patterns along with the contour fields of the vorticity, as well as the air entrapped by the ship section for the grid size 1×10^{-3} m. Fig. 20 show the time history of the velocity

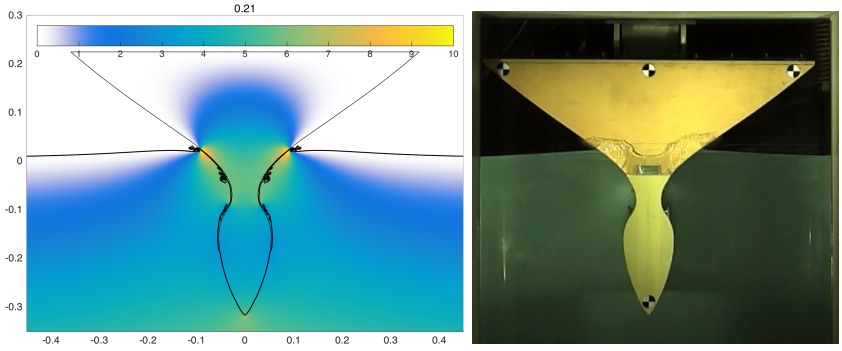

(a) Pressure distribution and free surface (b) Experiment [40]

Figure 18: Water impact problem (case 2) at $t = 0.21$.

under mesh refinement. The velocity agrees well with the experimental data. Fig. 21 show the pressure distribution and the corresponding snapshot of the experiment.

Table 5: Description of four grids employed in the water impact problem for case 3.

n	Δx (m)	grid size
1	8×10^{-3}	192×144
2	4×10^{-3}	384×288
3	2×10^{-3}	768×576
4	1×10^{-3}	1536×1152

In summary, the numerical tests show that the proposed one fluid formulation can simulate very challenging problem involving the impact of the structure and wave-breaking. We highlight the method to resolve the pressure distribution on the complex geometry such as a ship section. Cubic spline interpolation is used to reduce the pressure oscillation.

6. Conclusion

This work has presented a one-fluid computational framework for the efficient computation of the wave interacting with floating body problem. This novel framework enables the modelling of the interaction problem into a one-fluid formulation. From the mathematical modelling point of view, this work has clearly shown what is the rigidity force imposed on the rigid body and proved the given formulation is equivalent to the traditional boundary fitted formulation.

Compared with other fictitious domain Lagrangian multiplier based method, we do not solve the linear and angular momentum balance equation for the rigid region, as it is already handled by the fluid solver. Instead, we proposed a cheap

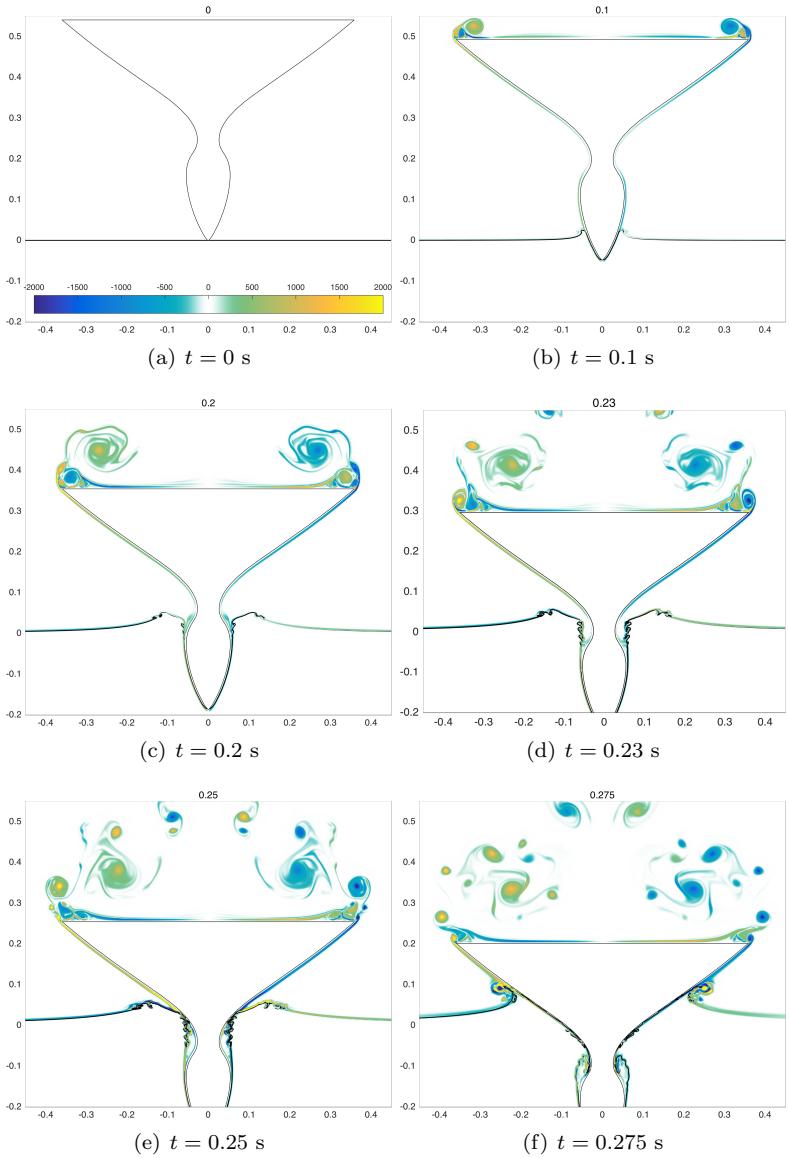

(a) $t = 0$ s (b) $t = 0.1$ s

(c) $t = 0.2$ s (d) $t = 0.23$ s

(e) $t = 0.25$ s (f) $t = 0.275$ s

Figure 19: Water impact problem (case 3): the air-water-rigid interface position (solid black line) and vorticity contours ($-2000 < \omega < 2000$), $dx = 1 \times 10^{-3}$ m.

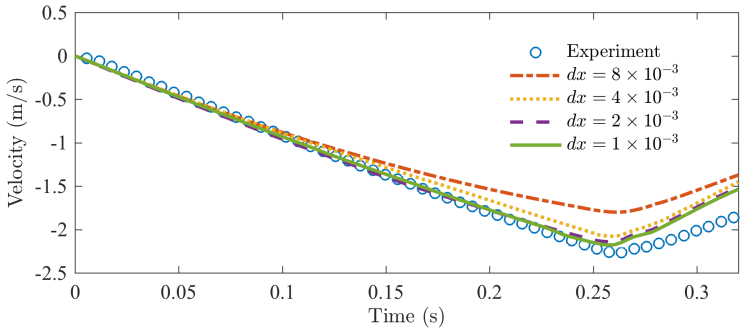

Figure 20: Water impact problem (case 3): time history of the velocity under mesh refinement, compared with the experimental data.

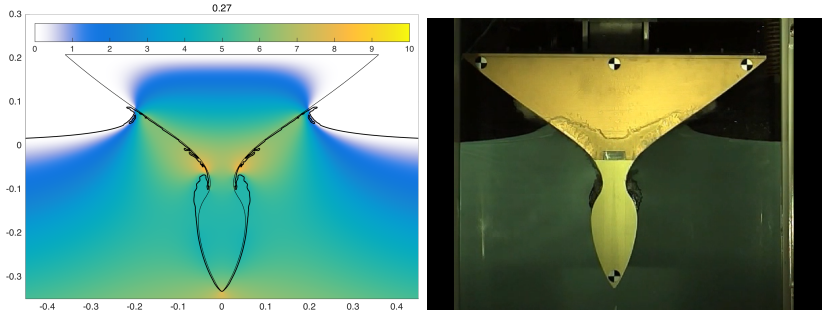

(a) Pressure distribution and free surface, $dx = 1 \times 10^{-3}$ m.

(b) Experiment [40]

Figure 21: Water impact problem (case 3) at $t = 0.27$ s.

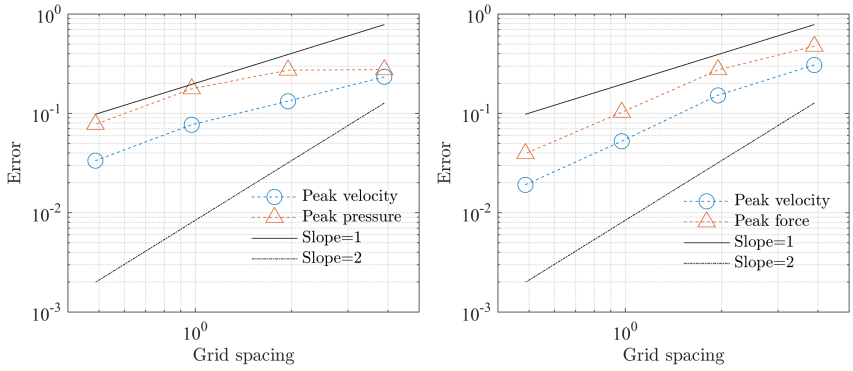

(a) Case 1

(b) Case 2

Figure 22: Water impact problem. Grid convergence of the peak velocity, peak pressure for case 1 and peak force for case 2.

linear least squares method from a pure kinetic point of view, which allowed different cases of rigid body motion.

A convolution procedure is introduced for the initialisation of the smoothed rigid Heaviside function from an arbitrary shape and an interpolation procedure for the movement the rigid Heaviside, which is much cheaper than the particle tracking and integration used by the immersed boundary methods. The accuracy of this methods depends on the spatial discretisation techniques, other than the number of the particles used. A high order interpolation scheme is used to reduce the force and pressure oscillation. Several examples have been carried out for validation of the present approach. The pressure are compared for the water impact problem with the recent experimental data.

References

[1] M. S. Longuet-Higgins and E. Cokelet. The deformation of steep surface waves on water. i. a numerical method of computation. In *Proceedings of the Royal Society of London A: Mathematical, Physical and Engineering Sciences*, volume 350, pages 1–26. The Royal Society, 1976.

[2] R. Panahi, E. Jahanbakhsh, and M. S. Seif. Development of a VoF-fractional step solver for floating body motion simulation. *Applied ocean research*, 28(3):171–181, 2006.

[3] R. B. Canelas, J. M. Domínguez, A. J. Crespo, M. Gómez-Gesteira, and R. M. Ferreira. A Smooth Particle Hydrodynamics discretization for the modelling of free surface flows and rigid body dynamics. *International Journal for Numerical Methods in Fluids*, 2015.

[4] P. Omidvar, P. K. Stansby, and B. D. Rogers. Wave body interaction in 2D using smoothed particle hydrodynamics (SPH) with variable particle mass. *International Journal for Numerical Methods in Fluids*, 68(6):686–705, 2012.

[5] H. H. Hu, N. A. Patankar, and M. Zhu. Direct numerical simulations of fluid–solid systems using the arbitrary Lagrangian–Eulerian technique. *Journal of Computational Physics*, 169(2):427–462, 2001.

[6] E. Walhorn, A. Kölke, B. Hübner, and D. Dinkler. Fluid-Structure coupling within a monolithic model involving free surface flows. *Computers and Structures*, 83(25-26):2100–2111, 2005.

[7] S. V. Apte, M. Martin, and N. A. Patankar. A numerical method for fully resolved simulation (FRS) of rigid particle–flow interactions in complex flows. *Journal of Computational Physics*, 228(8):2712–2738, 2009.

[8] J. Yang and F. Stern. A non-iterative direct forcing immersed boundary method for strongly-coupled fluid–solid interactions. *Journal of Computational Physics*, 295:779–804, 2015.

[9] T. Belytschko, Y. Krongauz, J. Dolbow, and C. Gerlach. On the completeness of meshfree particle methods. *International Journal for Numerical Methods in Engineering*, 43(5):785–819, 1998.

[10] C. S. Peskin. Flow patterns around heart valves: A numerical method. *Journal of Computational Physics*, 10(2):252–271, 1972.

[11] R. Mittal and G. Iaccarino. Immersed boundary methods. *Annual Review of Fluid Mechanics*, 37(1):239–261, 2005.

[12] M. Uhlmann. An immersed boundary method with direct forcing for the simulation of particulate flows. *Journal of Computational Physics*, 209(2):448–476, 2005.

[13] Z. Yu and X. Shao. A direct-forcing fictitious domain method for particulate flows. *Journal of Computational Physics*, 227(1):292–314, 2007.

[14] H. S. Yoon, C. H. Jeon, J. H. Jung, B. Koo, C. Choi, and S. C. Shin. Simulation of two-phase flow–body interaction problems using direct forcing/fictitious domain–level set method. *International Journal for Numerical Methods in Fluids*, 73(3):250–265, 2013.

[15] J. Sanders, J. E. Dolbow, P. J. Mucha, and T. A. Laursen. A new method for simulating rigid body motion in incompressible two-phase flow. *International Journal for Numerical Methods in Fluids*, 67(6):713–732, 2011.

[16] A. Calderer, S. Kang, and F. Sotiropoulos. Level set immersed boundary method for coupled simulation of air/water interaction with complex floating structures. *Journal of Computational Physics*, 277:201–227, 2014.

[17] N. A. Patankar, P. Singh, D. D. Joseph, R. Glowinski, and T. W. Pan. A new formulation of the distributed Lagrange multiplier/fictitious domain method for particulate flows. *International Journal of Multiphase Flow*, 26(9):1509–1524, 2000.

[18] R. Glowinski, T. W. Pan, T. I. Hesla, D. D. Joseph, and J. Priaux. A fictitious domain approach to the direct numerical simulation of incompressible viscous flow past moving rigid bodies: Application to particulate flows. *Journal of Computational Physics*, 169(2):363–426, 2001.

[19] N. Sharma and N. A. Patankar. A fast computation technique for the direct numerical simulation of rigid particulate flows. *Journal of Computational Physics*, 205(2):439–457, 2005.

[20] J. Yang and F. Stern. A sharp interface direct forcing immersed boundary approach for fully resolved simulations of particulate flows. *Journal of Fluids Engineering*, 136(4):040904, 2014.

[21] G. Tryggvason, R. Scardovelli, and S. Zaleski. *Direct numerical simulations of gas-liquid multiphase flows*. Cambridge University Press, 2011.

[22] L. Yang. *An immersed computational framework for multiphase fluid-structure interaction*. PhD thesis, Swansea University, 2015.

[23] N. Patankar. A formulation for fast computations of rigid particulate flows. *Center for Turbulence Research Annual Research Briefs*, 2001:185–196, 2001.

[24] N. A. Patankar. Physical interpretation and mathematical properties of the stress-DLM formulation for rigid particulate flows. *International Journal for Computational Methods in Engineering Science and Mechanics*, 6(2):137–143, 2005.

[25] A. Prosperetti and G. Tryggvason. *Computational Methods for Multiphase Flows*. Cambridge University Press, 2007.

[26] S. Osher and J. Sethian. Fronts propagating with curvature-dependent speed: algorithms based on Hamilton-Jacobi formulations. *Journal of Computational Physics*, 79(1):12–49, 1988.

[27] M. Sussman, P. Smereka, and S. Osher. A Level Set Approach for Computing Solutions to Incompressible Two-Phase Flow. *Journal of Computational Physics*, 114(1):146–159, 1994.

[28] C. S. Peskin. Numerical analysis of blood flow in the heart. *Journal of Computational Physics*, 25(3):220–252, 1977.

[29] C. S. Peskin and D. M. McQueen. Modeling prosthetic heart valves for numerical analysis of blood flow in the heart. *Journal of Computational Physics*, 37(1):113–132, 1980.

[30] A. M. Roma, C. S. Peskin, and M. J. Berger. An adaptive version of the immersed boundary method. *Journal of Computational Physics*, 153(2):509–534, 1999.

[31] X. Yang, X. Zhang, Z. Li, and G.-W. He. A smoothing technique for discrete delta functions with application to immersed boundary method in moving boundary simulations. *Journal of Computational Physics*, 228(20):7821–7836, 2009.

[32] A. J. Gil, A. Arranz Carreño, J. Bonet, and O. Hassan. An enhanced Immersed Structural Potential Method for fluid-structure interactions. *Journal of Computational Physics*, 250(0):178–205, 2013.

[33] R. D. Falgout and U. M. Yang. hypre: A library of high performance preconditioners. In *Computational Science-ICCS 2002*, pages 632–641. Springer, 2002.

[34] K. Kleefsman, G. Fekken, A. Veldman, B. Iwanowski, and B. Buchner. A Volume-Of-Fluid based simulation method for wave impact problems. *Journal of Computational Physics*, 206(1):363–393, 2005.

[35] P. Lin. A fixed-grid model for simulation of a moving body in free surface flows. *Computers & Fluids*, 36(3):549–561, 2007.

[36] J. Yang and F. Stern. Sharp interface Immersed-Boundary Level-Set Method for wave body interactions. *Journal of Computational Physics*, 228(17):6590–6616, 2009.

[37] S. Itō. *Study of the transient heave oscillation of a floating cylinder.* PhD thesis, Massachusetts Institute of Technology, 1977.

[38] K. H. Jung, K.-A. Chang, and H. J. Jo. Viscous effect on the roll motion of a rectangular structure. *Journal of engineering mechanics*, 132(2):190–200, 2006.

[39] K. H. Jung, K.-A. Chang, and E. T. Huang. Two-dimensional flow characteristics of wave interactions with a free-rolling rectangular structure. *Ocean Engineering*, 32(1):1–20, 2005.

[40] Moeri. Wave induced loads on ships-joint industry project III. Technical report, Korea Research Institute of Ships and Ocean Engineering, 2013.

Lemma 1. *The two kinematic constraints for a velocity field* $\boldsymbol{u}$ *for a rigid body motion*

$$\boldsymbol{D}(\boldsymbol{u}) = \boldsymbol{0}$$

$$\boldsymbol{u} = \boldsymbol{U} + \boldsymbol{\omega} \times \boldsymbol{x}$$

are equivalent.

Proof. Let us assume that the velocity can be written as $\boldsymbol{u} = \boldsymbol{U} + \boldsymbol{\omega} \times \boldsymbol{x}$ such that

$$\boldsymbol{u} = \boldsymbol{U} + \boldsymbol{\omega} \times \boldsymbol{x} = \boldsymbol{U} + \begin{pmatrix} \omega_2 x_3 - \omega_3 x_2 \\ \omega_3 x_1 - \omega_1 x_3 \\ \omega_1 x_2 - \omega_2 x_1 \end{pmatrix}$$

Therefore,

$$\boldsymbol{\nabla u} = \begin{pmatrix} 0 & -\omega_3 & \omega_2 \\ \omega_3 & 0 & -\omega_1 \\ -\omega_2 & \omega_1 & 0 \end{pmatrix}$$

and hence,

$$\boldsymbol{D}(\boldsymbol{u}) = \frac{1}{2}(\boldsymbol{\nabla u} + (\boldsymbol{\nabla u})^T) = \boldsymbol{0}$$

Conversely, let us assume that. at a given time, $\boldsymbol{D}(\boldsymbol{u}) = \boldsymbol{0}$. Define the rotation rate tensor as $\boldsymbol{R}(\boldsymbol{u}) = \frac{1}{2}(\boldsymbol{\nabla u} - (\boldsymbol{\nabla u})^T)$, then we have property that

$$\boldsymbol{\nabla u} = \boldsymbol{D}(\boldsymbol{u}) + \boldsymbol{R}(\boldsymbol{u})$$

The gradient of the rotation rate tensor can be written in each component i, j, k definition of the $\boldsymbol{\nabla R}$ each components

$$\begin{aligned} \nabla R_{ij,l} &= \frac{1}{2}(u_{i,jl} - u_{j,il}) \\ &= \frac{1}{2}(u_{i,jl} + u_{l,ij} - u_{l,ij} - u_{j,il}) \\ &= \frac{1}{2}(d(u)_{il,j} - d(u)_{jl,i}) \\ &= 0 \end{aligned} \tag{.1}$$

It can be observed that $\boldsymbol{R}(\boldsymbol{u})$ is constant in space and so is $\boldsymbol{R}(\boldsymbol{u}) = \boldsymbol{D}(\boldsymbol{u}) - \boldsymbol{\nabla u}$. Using $\boldsymbol{D}(\boldsymbol{u}) = \boldsymbol{0}$.

$$\boldsymbol{\nabla u} = \boldsymbol{R}(\boldsymbol{u}) = constant$$

Note that $\boldsymbol{R}(\boldsymbol{u}) = -\boldsymbol{R}(\boldsymbol{u})^T$, $\boldsymbol{\nabla u}$ should have the following form:

$$\boldsymbol{\nabla u} = \begin{pmatrix} \frac{\partial u}{\partial x} & \frac{\partial u}{\partial y} & \frac{\partial u}{\partial z} \\ \frac{\partial v}{\partial x} & \frac{\partial v}{\partial y} & \frac{\partial v}{\partial z} \\ \frac{\partial w}{\partial x} & \frac{\partial w}{\partial y} & \frac{\partial w}{\partial z} \end{pmatrix} = \begin{pmatrix} 0 & -\omega_3 & \omega_2 \\ \omega_3 & 0 & -\omega_1 \\ -\omega_2 & \omega_1 & 0 \end{pmatrix}$$

where ω_i is constant in space. It follows by integration that

$$\boldsymbol{u} = \begin{pmatrix} U_1 - \omega_3 y + \omega_2 z \\ U_2 + \omega_3 y - \omega_1 z \\ U_3 - \omega_2 x + \omega_2 y \end{pmatrix}$$

so the velocity can be written in the form

$$\boldsymbol{u} = \boldsymbol{U} + \boldsymbol{\omega} \times \boldsymbol{x}$$

□

Lemma 2. *The continuum with rigid body kinematic constraints Eqs. (.2) is equivalent to the Newton-Euler equation Eqs. (.3) Newton-Euler formulation:*

$$\boldsymbol{u} = \boldsymbol{U} + \boldsymbol{\omega} \times \boldsymbol{x}, \qquad \textit{motion constraint, balance of mass} \tag{.2a}$$

$$\frac{d}{dt}\int_\Omega \rho \boldsymbol{u}\, dv = \int_\Omega \rho \boldsymbol{g}\, dv + \int_{\partial\Omega} \boldsymbol{t}\, da; \qquad \textit{balance of linear momentum} \tag{.2b}$$

$$\boldsymbol{\sigma} = \boldsymbol{\sigma}^T, \qquad \textit{balance of angular momentum} \tag{.2c}$$

where $\boldsymbol{t} = \boldsymbol{\sigma n}$ is the traction vector, $\boldsymbol{g}$ represents the gravitational acceleration.

$$M\frac{d\boldsymbol{u}_c}{dt} = \boldsymbol{f}_c; \qquad \textit{motion of centre of mass} \tag{.3a}$$

$$\boldsymbol{J}\frac{d\boldsymbol{\omega}}{dt} + \boldsymbol{\omega} \times \boldsymbol{J\omega} = \boldsymbol{t}_c, \qquad \textit{angular motion of rigid body} \tag{.3b}$$

where the M, $\boldsymbol{J}$ $\boldsymbol{\omega}$, $\boldsymbol{u}_c$, $\boldsymbol{f}_c$ and $\boldsymbol{t}_c$ are the mass, inertia tensor, angular velocity, centre mass velocity, force and torque applied on the rigid object, respectively.

Proof. To start with, we can change the rigid body motion reference to the centre of gravity $\boldsymbol{x}_c$, and write the Eq. (.2a) as

$$\boldsymbol{u} = \boldsymbol{u}_c + \boldsymbol{\omega} \times \boldsymbol{r}$$

where $\boldsymbol{r} = \boldsymbol{x} - \boldsymbol{x}_c$ and $\boldsymbol{u}_c = \boldsymbol{U} + \boldsymbol{\omega} \times \boldsymbol{x}_c$.

If the $\partial\Omega$ is chosen to be the exact boundary of the rigid body In Eq. (.2b) and substitute the above equation, we have

$$\begin{aligned}
&\frac{\mathrm{d}}{\mathrm{d}t}\int_\Omega \rho\boldsymbol{u}\, dv \\
=&\frac{\mathrm{d}}{\mathrm{d}t}\int_\Omega \rho(\boldsymbol{\omega}\times\boldsymbol{r}+\boldsymbol{u}_c)\, dv \\
=&\cancel{\frac{\mathrm{d}}{\mathrm{d}t}\int_\Omega \rho(\boldsymbol{\omega}\times\boldsymbol{r})\, dv}^{[3]} + \frac{\mathrm{d}}{\mathrm{d}t}\int_\Omega \rho\boldsymbol{u}_c\, dv \\
=&\int_\Omega \rho\, dv \frac{\mathrm{d}\boldsymbol{u}_c}{\mathrm{d}t} \\
=&M\frac{\mathrm{d}\boldsymbol{u}_c}{\mathrm{d}t}.
\end{aligned} \tag{.4}$$

where the mass of the rigid body is defined as

$$M = \int_\Omega \rho\, dv. \tag{.5}$$

On the right hand side of Eq. (.2b), the force applied on the rigid body can be written as

$$\boldsymbol{f}_c = \int_\Omega \rho\boldsymbol{g}\, dv + \int_{\partial\Omega} \boldsymbol{t}\, da. \tag{.6}$$

Here, now we have the Eq. (.3a) for the Newton-Euler equations.

□

Because of the symmetry of the Cauchy stress tensor Eq. (.2c), the angular momentum conservation equation is automatically satisfied. Let us consider the rotational equilibrium of a general body under the action of traction and body forces. This implies

$$\frac{\mathrm{d}}{\mathrm{d}t}\int_\Omega (\boldsymbol{r}\times\rho\boldsymbol{u})\, dv = \int_\Omega (\boldsymbol{r}\times\rho\boldsymbol{g})\, dv + \int_{\partial\Omega} (\boldsymbol{r}\times\boldsymbol{t})\, da. \tag{.7}$$

[3] From the definition of the gravitational centre, we have $\int_\Omega \rho r_i\, dv = 0$ for $i = 1, 2, 3$. Thus, $\int_\Omega \rho(\omega \times r)_i\, dv = \mathcal{E}_{ijk}\omega_j \int_\Omega (\rho r)_k = 0$

Similarly, substitution of $\boldsymbol{u} = \boldsymbol{u}_c + \boldsymbol{\omega} \times \boldsymbol{r}$ into the left hand side of Eq. (.7)

$$
\begin{aligned}
&\frac{\mathrm{d}}{\mathrm{d}t} \int_\Omega \boldsymbol{r} \times \rho \boldsymbol{u}(\boldsymbol{x}, t)\, dv \\
=&\int_\Omega \rho \boldsymbol{r} \times \frac{\mathrm{d}\boldsymbol{u}(\boldsymbol{x}, t)}{\mathrm{d}t}\, dv \quad \text{pullback and pushforward operation} \\
=&\int_\Omega \rho \boldsymbol{r} \times \frac{\mathrm{d}(\boldsymbol{\omega} \times \boldsymbol{r} + \boldsymbol{u}_c)}{\mathrm{d}t}\, dv \\
&\text{From } \int_\Omega \rho r_i\, dv = 0 \text{ for } i = 1, 2, 3, \text{ thus, } \int_\Omega (\rho r \times \frac{\mathrm{d}u_c}{\mathrm{d}t})_i\, dv = \mathcal{E}_{ijk} (\frac{\mathrm{d}u_c}{\mathrm{d}t})_k \int_\Omega (\rho r)_j\, dv = 0 \\
=&\int_\Omega \rho \boldsymbol{r} \times \frac{\mathrm{d}(\boldsymbol{\omega} \times \boldsymbol{r})}{\mathrm{d}t}\, dv + \cancel{\int_\Omega \rho \boldsymbol{r} \times \frac{\mathrm{d}\boldsymbol{u}_c}{\mathrm{d}t}\, dv} \\
&\text{Applying the chain rule} \\
=&\int_\Omega \rho \boldsymbol{r} \times (\frac{\mathrm{d}\boldsymbol{\omega}}{\mathrm{d}t} \times \boldsymbol{r})\, dv + \int_\Omega \rho \boldsymbol{r} \times (\boldsymbol{\omega} \times \frac{\mathrm{d}\boldsymbol{r}}{\mathrm{d}t})\, dv \\
&\text{Using } \frac{\mathrm{d}\boldsymbol{r}}{\mathrm{d}t} = \boldsymbol{\omega} \times \boldsymbol{r} \\
=&\int_\Omega \rho \boldsymbol{r} \times (\frac{\mathrm{d}\boldsymbol{\omega}}{\mathrm{d}t} \times \boldsymbol{r})\, dv + \int_\Omega \rho \boldsymbol{r} \times [\boldsymbol{\omega} \times (\boldsymbol{\omega} \times \boldsymbol{r})]\, dv \\
=&\int_\Omega \rho(|\boldsymbol{r}|^2 \boldsymbol{I} - \boldsymbol{r} \otimes \boldsymbol{r}) \frac{\mathrm{d}\boldsymbol{\omega}}{\mathrm{d}t}\, dv + \int_\Omega \rho \boldsymbol{\omega} \times [(|\boldsymbol{r}|^2 \boldsymbol{I} - \boldsymbol{r} \otimes \boldsymbol{r})\boldsymbol{\omega}]\, dv \\
=&\boldsymbol{J} \frac{\mathrm{d}\boldsymbol{\omega}}{\mathrm{d}t} + \boldsymbol{\omega} \times \boldsymbol{J}\boldsymbol{\omega}.
\end{aligned}
$$

where the inertia tensor of the rigid body is defined as

$$\boldsymbol{J} = \int_\Omega \rho(|\boldsymbol{r}|^2 \boldsymbol{I} - \boldsymbol{r} \otimes \boldsymbol{r})\, dv. \tag{.8}$$

On the right hand side of Eq. (.7), the torque applied on the rigid body can be written as

$$\boldsymbol{t}_c = \int_\Omega \boldsymbol{r} \times \rho \boldsymbol{g}\, dv + \int_{\partial\Omega} \boldsymbol{r} \times \boldsymbol{t}\, da. \tag{.9}$$

Here we have the angular momentum Eq. (.3b) for the Newton-Euler equations.

Lemma 3. *The one-fluid equation is equivalent to the separated governing equation with the interface condition.*

Proof. The one-fluid conservation of the mass equation

$$\int_\Omega \frac{\partial \rho}{\partial t}\, dv + \int_{\partial\Omega} \rho \boldsymbol{u}\, da = 0$$

Assuming there is no mass change on the interface, we have the Ranine-Hugoniot jump condition (Lemma 4)

$$c\, [\![\rho]\!] = [\![\rho \boldsymbol{u}]\!] \cdot \boldsymbol{n}; \quad \rho_1(\boldsymbol{u}_1 \cdot \boldsymbol{n} - c) = \rho_2(\boldsymbol{u}_2 \cdot \boldsymbol{n} - c)$$

For incompressibility, this equation $\rho_1(\boldsymbol{u}_1 \cdot \boldsymbol{n} - c) = \rho_2(\boldsymbol{u}_2 \cdot \boldsymbol{n} - c)$ must be hold for arbitrary density ratios, the only condition is $\boldsymbol{u}_1 \cdot \boldsymbol{n} = \boldsymbol{u}_2 \cdot \boldsymbol{n}$. There is no restriction for the tangential velocity. However, a slip on the tangential will result indefinite stresses. Thus, the kinematic boundary condition is

$$[\![\boldsymbol{u}]\!] = \boldsymbol{0}$$

The conservation of the linear momentum in a conservative manner

$$\int_\Omega \frac{\partial(\rho \boldsymbol{u})}{\partial t}\, dv + \int_{\partial\Omega} (\rho \boldsymbol{u} \otimes \boldsymbol{u} - \boldsymbol{\sigma})\, da = \int_\Omega \rho \boldsymbol{g}\, dv$$

This one-fluid equation will lead to a jump condition one the interface Γ

$$c\,[\![\rho \boldsymbol{u}]\!] = [\![\rho \boldsymbol{u} \otimes \boldsymbol{u} - \boldsymbol{\sigma}]\!]\, \boldsymbol{n};$$

In the case of incompressibility, using the kinematic interface condition, the dynamic interface condition becomes

$$[\![\boldsymbol{\sigma}]\!]\, \boldsymbol{n} = \boldsymbol{0}$$

So we have

$$\boldsymbol{\sigma}_r \boldsymbol{n} = \boldsymbol{\sigma}_f \boldsymbol{n} = \mu \frac{\partial \boldsymbol{u}_f}{\partial n} - p\boldsymbol{n}$$

Above equation the implicit dynamic B.C. for the one-fluid formulation. In order to compared with the separated governing equation, apply it to the rigid body Ω_r,

$$\frac{\mathrm{d}}{\mathrm{d}t} \int_{\Omega_r} \rho \boldsymbol{u}\, dv = \int_{\Omega_r} \rho \boldsymbol{g}\, dv + \int_{\partial\Omega_r} \boldsymbol{t}\, da$$

where $\boldsymbol{t} = \boldsymbol{\sigma}_r \boldsymbol{n} = \mu \frac{\partial \boldsymbol{u}_f}{\partial n} - p\boldsymbol{n}$. Using Lemma 2, above equation is simplified into

$$M \frac{\mathrm{d}\boldsymbol{u}_c}{\mathrm{d}t} = M\boldsymbol{g} + \int_{\partial\Omega_r} (\mu \frac{\partial \boldsymbol{u}_f}{\partial n} - p\boldsymbol{n})\, da$$

which is the Newton-Euler equation with dynamic boundary condition. Similar procedure can be applied to the angular momentum equation. □

Lemma 4. *Suppose that we have a fixed domain $\Omega \subset \mathbb{R}^{2,3}$ which is divided into two subdomain Ω_1 and Ω_2 by a single propagating discontinuity on a surface Γ, associated with the conservation law*

$$\frac{d}{dt} \int_\Omega \phi\, dv + \int_{\partial\Omega} \mathbf{F}\boldsymbol{n}\, da = \int_\Omega f\, dv \tag{.10}$$

We will assume that the normal $\boldsymbol{n}$ to the discontinuity is oriented to the point from Ω_1 to Ω_2. At any point on the discontinuity surface, let ϕ_1 and ϕ_2 be the values of ϕ as we approach the point from inside Ω_1 and Ω_2, respectively. Similarly, let $\mathbf{F}_1$ and $\mathbf{F}_2$ be the values of $\mathbf{F}$ associated with the two domains on either side of the discontinuity. Finally, let c is the normal component of the

velocity of the discontinuity. Then the **Ranine-Hugoniot Jump Condition** *holds:*

$$c\,[\![\phi]\!] = [\![\mathbf{F}(\phi)]\!]\,\boldsymbol{n}, \tag{.11}$$

the jump of the variable ϕ across the surface is defined as $[\![\phi]\!] = \phi_1 - \phi_2$, where ϕ_1 and ϕ_2 are the variable values on each side of the surface.

Proof. If $\boldsymbol{u}(\boldsymbol{x})$ is the velocity at a point $\boldsymbol{x}$ on the discontinuity surface, then the formulas for the derivative of an integral leads to the equations

$$\frac{d}{dt}\int_{\Omega_1} \phi\, dv = \int_{\Omega_1} \frac{\partial \phi}{\partial t}\, dv + \int_{\Gamma} \phi_1 \boldsymbol{n}\cdot\boldsymbol{u}\, da$$

and

$$\frac{d}{dt}\int_{\Omega_2} \phi\, dv = \int_{\Omega_2} \frac{\partial \phi}{\partial t}\, dv - \int_{\Gamma} \phi_2 \boldsymbol{n}\cdot\boldsymbol{u}\, da$$

Away from the discontinuity surface, the conservation law can be written as the PDE

$$\frac{\partial \phi}{\partial t} + \boldsymbol{\nabla}\cdot\mathbf{F}(\phi) = f(\boldsymbol{x}, t),$$

We use the fact that $\boldsymbol{n}\cdot\boldsymbol{u} = c$ is the normal speed of the discontinuity to get

$$\begin{aligned}
\frac{d}{dt}\int_{\Omega} \phi\, dv &= \frac{d}{dt}\int_{\Omega_1} \phi\, dv + \frac{d}{dt}\int_{\Omega_2} \phi\, dv \\
&= \int_{\Omega_1} \frac{\partial \phi}{\partial t}\, dv + \int_{\Gamma} \phi_1 \boldsymbol{n}\cdot\boldsymbol{u}\, da + \int_{\Omega_2} \frac{\partial \phi}{\partial t}\, dv - \int_{\Gamma} \phi_2 \boldsymbol{n}\cdot\boldsymbol{u}\, da \\
&= \int_{\Omega_1} (f - \boldsymbol{\nabla}\cdot\mathbf{F})\, dv + \int_{\Gamma} \phi_1 \boldsymbol{n}\cdot\boldsymbol{u}\, da + \int_{\Omega_2} (f - \boldsymbol{\nabla}\cdot\mathbf{F})\, dv - \int_{\Gamma} \phi_2 \boldsymbol{n}\cdot\boldsymbol{u}\, da
\end{aligned}$$

then we apply the divergence theorem to get

$$= \int_{\partial\Omega_1} f\, dv - \int_{\partial\Omega_1} \mathbf{F}\boldsymbol{n}\, da + \int_{\partial\Omega_2} f\, dv - \int_{\partial\Omega_2} \mathbf{F}\boldsymbol{n}\, da - \int_{\Gamma} c\,[\![\phi]\!]\, da$$

we use the fact that $\partial\Omega_1 \cup \partial\Omega_2 = \Omega \cup \Gamma$ to get

$$= \int_{\Omega} f\, dv - \int_{\partial\Omega} \mathbf{F}\boldsymbol{n}\, da + \int_{\Gamma} [\![\mathbf{F}(\phi)]\!]\,\boldsymbol{n}\, da - \int_{\Gamma} c\,[\![\phi]\!]\, da$$

Subtracting the original form (.11) for the conservation law, we obtain

$$\int_{\Gamma} [\![\mathbf{F}(\phi)]\!]\,\boldsymbol{n}\, da = \int_{\Gamma} c\,[\![\phi]\!]\, da$$

By shrinking the Γ and Ω around a point, we obtain the Ranine-Hugoniot jump condition (.10). □

This lemma says that the jump in the normal component of the flux is equal to the jump in the conserved quantities times the normal velocity of the discontinuity.